

ENCLOSURE 7

TENNESSEE VALLEY AUTHORITY
BROWNS FERRY NUCLEAR PLANT (BFN)
UNITS 1, 2, AND 3

TECHNICAL SPECIFICATIONS (TS) CHANGES TS-431 AND TS-418
EXTENDED POWER UPRATE (EPU)

CDI REPORT NO. 08-07NP, "STRESS ASSESSMENT OF BROWNS FERRY
NUCLEAR UNIT 2 STEAM DRYER"

(NON-PROPRIETARY VERSION)

Attached is the **Non-Proprietary Version** of CDI Report No. 08-07,
"Stress Assessment of Browns Ferry Nuclear Unit 2 Steam Dryer."

Stress Assessments of Browns Ferry Nuclear
Unit 2 Steam Dryer

Revision 1

Prepared by

Continuum Dynamics, Inc.
34 Lexington Avenue
Ewing, NJ 08618

Prepared under Purchase Order No. 00053157 for

TVA / Browns Ferry Nuclear Plant
Nuclear Plant Road, P. O. Box 2000 PAB-2M
Decatur, AL 35609

Approved by



Alan J. Bilanin

Reviewed by



Milton E. Teske
April 2008

This report complies with Continuum Dynamics, Inc. Nuclear Quality Assurance Program currently in effect.

Executive Summary

The finite element model and analysis methodology used to assess stresses induced by the flow of steam through the steam dryer at Brown Ferry Nuclear Unit 2 (BFN2), are described and applied to obtain stresses at CLTP conditions. The analysis is carried out in the frequency domain, which confers a number of useful computational advantages over a time accurate transient analysis including the ability to assess the effects of frequency scalings in the loads without the need for additional finite element calculations. [[

(3)]]

The analysis begins by developing a series of unit stress solutions corresponding to the application of a unit pressure at a MSL at specified frequency, f . Each unit solution is obtained by first calculating the associated acoustic pressure field using a separate analysis that solves the damped Helmholtz equation within the steam dryer [1]. This pressure field is then applied to a finite element structural model of the steam dryer and the harmonic stress response at frequency, f , calculated using the commercial ANSYS 10.0 finite element analysis software. This stress response constitutes the unit solution and is stored as a file for subsequent processing. Once all unit solutions have been computed, the stress response for any combination of MSL pressure spectrums (obtained by fast Fourier transform of the pressure histories in the MSLs) is determined by a simple matrix multiplication of these spectrums with the unit solutions.

This report provides details of the ANSYS 10.0 finite element structural model of the BFN2 steam dryer and reviews pertinent modeling considerations. It also summarizes the framework underlying the development and application of unit solutions in the frequency domain and shows how these solutions are used to develop stress histories for general load conditions. Next, it reviews the assessment of these stresses for compliance with the ASME B&PV Code, Section III, subsection NG, for the load combination corresponding to normal operation (the Level A Service Condition). [[

(3)]]

Results obtained from application of the methodology to the BFN2 steam dryer show that at nominal CLTP operation the minimum alternating stress ratio (SR-a) anywhere on the steam dryer is $SR-a=2.35$. The loads used to obtain this value account for all the end-to-end biases and uncertainties in the loads model [2] and finite element analysis. In order to account for uncertainties in the modal frequency predictions of the finite element model, the stresses are also computed for loads that are shifted in the frequency domain by $\pm 2.5\%$, $\pm 5\%$, $\pm 7.5\%$ and $\pm 10\%$. The minimum alternating stress ratio encountered at any frequency shift is found to be $SR-a=1.65$ occurring at the $+10\%$ shift. The stress ratio due to maximum stresses (SR-P) is dominated by static loads and is $SR-P=1.82$ without frequency shifts and $SR-P=1.75$ when frequency shifts are considered. Given the high alternating stress ratio SR-a and the comparatively small dependence of SR-P upon acoustic loads, these values are expected to qualify the Unit 2 dryer at EPU conditions.

Revision Summary

The following changes were implemented from Revision 0 to Revision 1:

- The last paragraph on page 72 was removed.
- Table 7 has been modified by: (i) adding Table 7c and (ii) changing the captions to indicate whether noise was filtered or not.
- Table 8 has been modified by: (i) adding Table 8c and (ii) changing the captions to indicate whether noise was filtered or not.
- Sentence referring to unfiltered CLTP loads for Unit 1 in Section "5. Results" has been removed. Additional tables presenting the stresses and stress ratios for unfiltered CLTP loads for Unit 2 have been added, together with references to these tables in the text.
- Pages have been renumbered to reflect changes and addition of tables.

Table of Contents

Section	Page
Executive Summary	i
Revision Summary	ii
Table of Contents	iii
1. Introduction and Purpose	1
2. Methodology	3
2.1 Overview	3
2.2 [[⁽³⁾]]	5
2.3 Computational Considerations	6
3. Finite Element Model Description	9
3.1 Steam Dryer Geometry	9
3.2 Material Properties	11
3.3 Model Simplifications	11
3.4 Perforated Plate Model	12
3.5 Vane Bank Model	13
3.6 Water Inertia Effect on Submerged Panels	14
3.7 Structural Damping	14
3.8 Mesh Details and Element Types	14
3.9 Connections Between Structural Components	15
3.10 Pressure Loading	25
4. Structural Analysis	28
4.1 Static Analysis	28
4.2 Harmonic Analysis	28
4.3 Post-Processing	33
4.4 Computation of Stress Ratios for Structural Assessment	33
5. Results	37
5.1 General Stress Distribution and High Stress Locations	38
5.2 Load Combinations and Allowable Stress Intensities	51
5.3 Frequency Content and Filtering of the Stress Signals	66
6. Conclusions	72
7. References	73

1. Introduction and Purpose

Plans to qualify the Browns Ferry nuclear plant for operation at Extended Power Uprate (EPU) operating condition require an assessment of the steam dryer stresses experienced under the increased loads. The steam dryer loads due to pressure fluctuations in the main steam lines (MSLs) are potentially damaging and the cyclic stresses from these loads can produce fatigue cracking if loads are sufficiently high. The industry has addressed this problem with physical modifications to the dryers, as well as a program to define steam dryer loads and their resulting stresses.

The purpose of the stress analysis discussed here is to calculate the maximum and alternating stresses generated during Current Licensed Thermal Power (CLTP) and determine the margins that exist when compared to stresses that comply with the ASME Code (ASME B&PV Code, Section III, subsection NG). This step establishes whether the modifications done prior to commercial operations are adequate for sustaining structural integrity and preventing future weld cracking under planned EPU operating conditions. The load combination considered here corresponds to normal operation (the Level A Service Condition) and includes fluctuating pressure loads developed from Browns Ferry Unit 2 (BFN2) main steam line data, and weight. The fluctuating pressure loads, induced by the flowing steam, are predicted using a separate acoustic circuit analysis of the steam dome and main steam lines [3]. Level B service conditions, which include seismic loads, are not included in this evaluation.

[[

⁽³⁾]] This approach also affords a number of additional computational advantages over transient simulations including: [[

⁽³⁾]] This last advantage is realized through the use of “unit” solutions representing the stress distribution resulting from the application of a unit fluctuating pressure at one of the MSLs at a particular frequency. [[
⁽³⁾]]

This report describes the overall methodology used to obtain the unit solutions in the frequency domain and how to assemble them into a stress response for a given combination of

pressure signals in the MSLs. This is followed by details of the BFN2 steam dryer finite element model including the elements used and overall resolution, treatment of connections between elements, the hydrodynamic model, the implementation of structural damping and key idealizations/assumptions inherent to the model. Post-processing procedures are also reviewed including the computation of maximum and alternating stress intensities, identification of high stress locations, adjustments to stress intensities at welds and evaluation of stress ratios used to establish compliance with the ASME Code. The results in terms of stress intensity distributions and stress ratios are presented next together with PSDs of the dominant stress components.

2. Methodology

2.1 Overview

Based on previous analysis undertaken at Quad Cities Units 1 and 2, the steam dryer can experience strong acoustic loads due to the fluctuating pressures in the MSLs connected to the steam dome containing the dryer. C.D.I. has developed an acoustic circuit model (ACM) that, given a collection of strain gage measurements [4] of the fluctuating pressures in the MSLs, predicts the acoustic pressure field anywhere inside the steam dome and on the steam dryer [1-3]. The ACM is formulated in frequency space and contains two major components that are directly relevant to the ensuing stress analysis of concern here. [[

(1)

(2)

⁽³⁾]]

[[

(3)

(4)

(5)

(3)]]

[[

(6)

(3)]]

2.2 [[
[[

(3)]]

(3)]]

[[

(3)]]

2.3 Computational Considerations

Focusing on the structural computational aspects of the overall approach, there are a number of numerical and computational considerations requiring attention. The first concerns the transfer of the acoustic forces onto the structure, particularly the spatial and frequency resolutions. The ANSYS finite element program inputs general distributed pressure differences using a table format. This consists of regular 3D rectangular (i.e., block) $n_x \times n_y \times n_z$ mesh where n_α is the number of mesh points in the i -th Cartesian direction and the pressure difference is provided at each mesh point (see Section 3.10). These tables are generated separately using a program that reads the loads provided from the ACM software, distributes these loads onto the finite element mesh using a combination of interpolation procedures on the surface and simple diffusion schemes off the surface (off-surface loads are required by ANSYS to ensure proper interpolation of forces), and written to ASCII files for input to ANSYS. A separate load file is written at each frequency for the real and imaginary component of the complex force.

The acoustic field is stored at 5 Hz intervals from 0 to 250 Hz. While a 5 Hz resolution is sufficient to capture frequency dependence of the acoustic field (i.e., the pressure at a point varies gradually with frequency), it is too coarse for representing the structural response especially at low frequencies. For 1% critical structural damping, one can show that the frequency spacing needed to resolve a damped resonant peak at natural frequency, f_n , to within 5% accuracy is $\Delta f = 0.0064 \times f_n$. Thus for $f_n = 10$ Hz where the lowest structural response modes occur, a frequency interval of 0.064 Hz or less is required. In our calculations we require that 5% maximum error be maintained over the range from $f_n = 5$ Hz to 250 Hz resulting in a finest frequency interval of 0.0321 Hz at the low frequency end (this adequately resolves all structural modes up to 250 Hz). Since there are no structural modes between 0 to 5 Hz, a 0.5 Hz spacing is used over this range with minimal (less than 5%) error. The unit load, $\hat{f}_n(\omega, \mathbf{R})$, at any frequency, ω_k , is obtained by linear interpolation of the acoustic solutions at the two nearest frequencies, ω_i and ω_{i+1} , spaced 5 Hz apart. Linear interpolation is sufficient since the pressure load varies slowly over the 5 Hz range (linear interpolation of the structural response would not be acceptable over this range since it varies much more rapidly over the same interval).

Solution Management

[[

(3)]]

[[

(3)]]

Structural Damping

In harmonic analysis one has a broader selection of damping models than in transient simulations. A damping factor, z , of 1% critical damping is used in the structural analysis. In transient simulations, this damping can only be enforced exactly at two frequencies (where the damping model is “pinned”). Between these two frequencies the damping factor can be considerably smaller, for example 0.5% or less depending on the pinning frequencies. Outside the pinning frequencies, damping is higher. With harmonic analysis it is straightforward to enforce very close to 1% damping over the entire frequency range. In this damping model, the damping matrix, \mathbf{D} , is set to

$$\mathbf{D} = \frac{2z}{\omega} \mathbf{K} \quad (7)$$

where \mathbf{K} is the stiffness matrix and ω the forcing frequency. One can show that with this model the damping factor varies between 0.995% and 1.005% which is a much smaller variation than using the pinned model required in transient simulation.

Load Frequency Rescaling

One way to evaluate the sensitivity of the stress results to approximations in the structural modeling and applied loads is to rescale the frequency content of the applied loads. In this procedure the nominal frequencies, ω_k , are shifted to $(1+\lambda)\omega_k$, where the frequency shift, λ , ranges between $\pm 10\%$, and the response recomputed for the shifted loads. The objective of the frequency shifting can be explained by way of example. Suppose that in the actual dryer a strong structural-acoustic coupling exists at a particular frequency, ω^* . This means that the following conditions hold simultaneously: (i) the acoustic signal contains a significant signal at ω^* ; (ii) the structural model contains a resonant mode of natural frequency, ω_n , that is near ω^* ; and (iii) the associated structural mode shape is strongly coupled to the acoustic load (i.e., integrating the product of the mode shape and the surface pressure over the steam dryer surface produces a significant modal force). Suppose now that because of discretization errors and modeling idealizations that the predicted resonance frequency differs from ω^* by a small amount (e.g., 1.5%). Then condition (ii) will be violated and the response amplitude therefore significantly

diminished. By shifting the load frequencies one re-establishes condition (ii) when $(1 + \lambda)\omega^*$ is near ω_n . The other two requirements also hold and a strong structural acoustic interaction is restored.

[[

(3)]]

Evaluation of Maximum and Alternating Stress Intensities

Once the unit solutions have been obtained, the most intensive computational steps in the generation of stress intensities are: (i) the FFTs to evaluate stress time histories from (5); and (ii) the calculation of alternating stress intensities. [[

(3)]]

The high computational penalty incurred in calculating the alternating stress intensities is due to the fact that this calculation involves comparing the stress tensors at every pair of points in the stress history. This comparison is necessary since in general the principal stress directions can vary during the response, thus for N samples in the stress history, there will be $(N-1)N/2$ such pairs or, for $N=64K$ (the number required to accurately resolve the spectrum up to 250 Hz in 0.01 Hz intervals), 2.1×10^9 calculations per node each requiring the determination of the roots to a cubic polynomial. [[

(3)]]

3. Finite Element Model Description

A description of the ANSYS model of the Browns Ferry Unit 2 steam dryer follows.

3.1 Steam Dryer Geometry

A geometric representation of the Browns Ferry Unit 2 steam dryer was developed from available drawings (provided by TVA and included in the design record file, DRF-TVA-250B) within the Workbench module of ANSYS. The completed model is shown in Figure 1. This model includes anticipated modifications to the Browns Ferry Unit 2 steam dryer. Namely, top tie rods are replaced with the thicker ones currently installed on Unit 1. The gussets on the top of the outer hoods supporting the steam dam plate were also cut away to facilitate installation of the new tie bars and possibly alleviate local stresses.

The modified areas are shown in Figure 2.

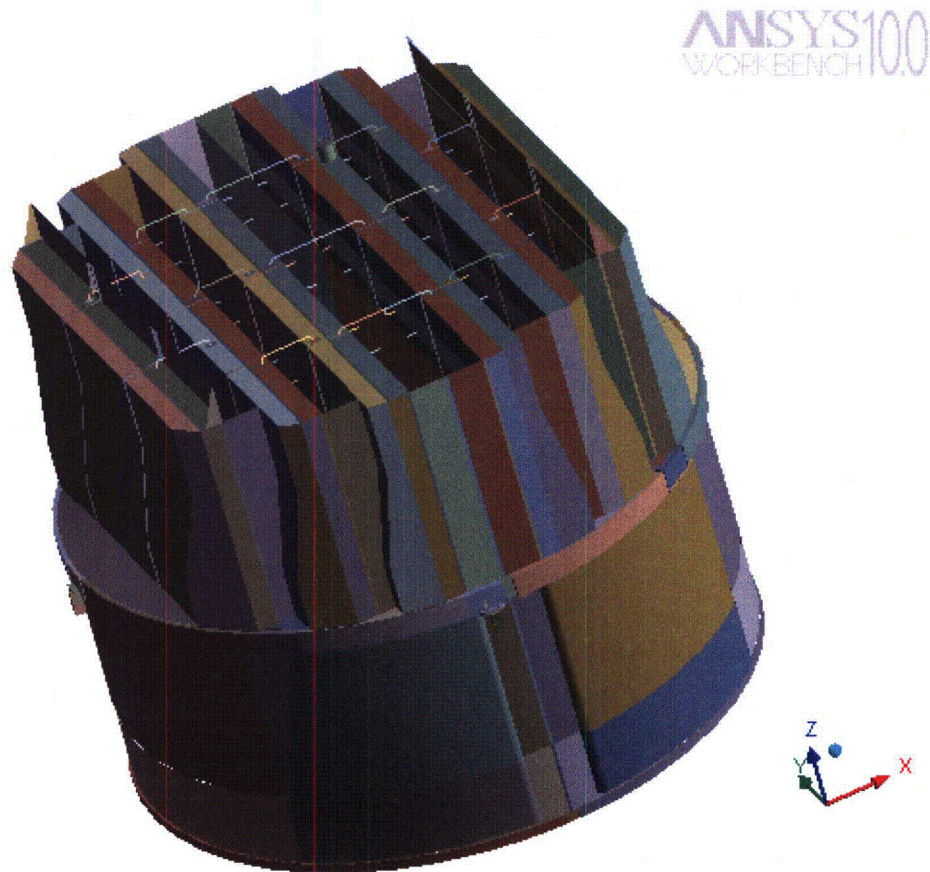


Figure 1. Overall geometry of the Browns Ferry Unit 2 steam dryer model.

Lock mechanisms
for new tie bars;
gussets are removed

New top tie bars are
installed

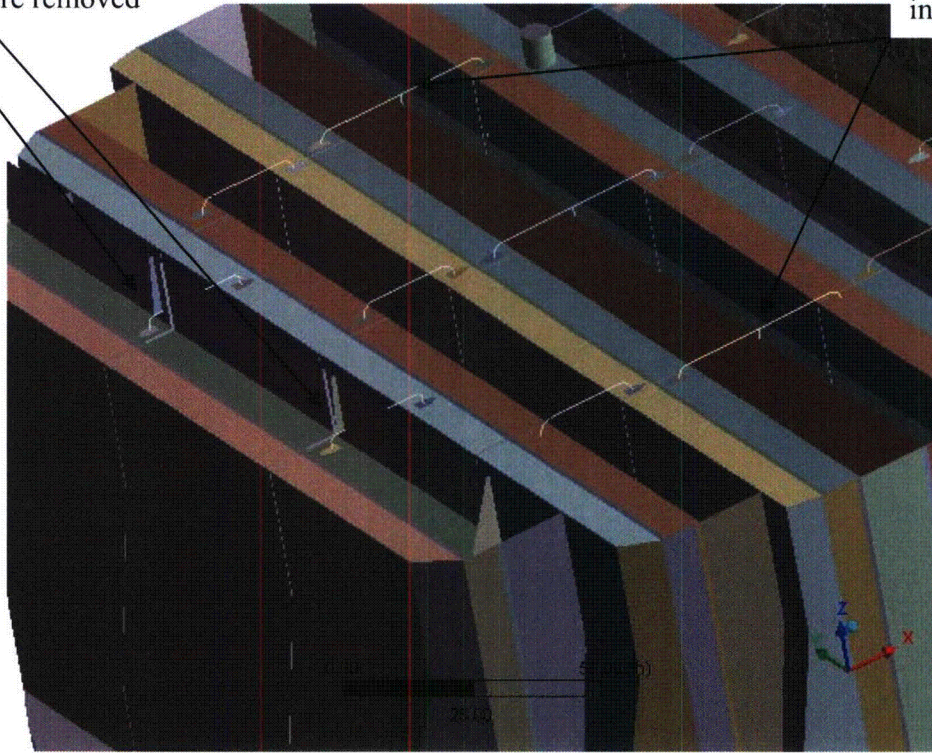


Figure 2. Anticipated modifications accounted for in the model and associated geometrical details.

3.2 Material Properties

The steam dryer is constructed from Type 304 stainless steel and has an operating temperature of 550°F. Properties used in the analysis are summarized below in Table 1.

Table 1. Material properties.

	Young's Modulus (10 ⁶ psi)	Density (lbm/in ³)	Poisson Ratio
Structural Steel	25.55	0.284	0.3
Structural Steel with Added Water Inertia Effect	25.55	1.055	0.3

The structural steel modulus is taken from Appendix A of the ASME Code for Type 304 Stainless Steel at an operating temperature 550°F. The effective properties of perforated plates and submerged parts are discussed in Sections 3.4 and 3.6. Note that the increased effective density for submerged components is only used in the harmonic analysis. When calculating the stress distribution due to the static dead weight load, the unmodified density of steel (0.284 lbm/in³) is used throughout.

3.3 Model Simplifications

The following simplifications were made to achieve reasonable model size while maintaining good modeling fidelity for key structural properties:

- Perforated plates were approximated as continuous plates using modified elastic properties designed to match the static and modal behaviors of the perforated plates. The perforated plate structural modeling is summarized in Section 3.4 and Appendix C of [6].
- The drying vanes were replaced by point masses attached to the corresponding trough bottom plates and vane bank top covers (Figure 4). The bounding perforated plates, vane bank end plates, and vane bank top covers were explicitly modeled (see Section 3.5).
- The added mass properties of the lower part of the skirt below the reactor water level were obtained using a separate hydrodynamic analysis (see Section 3.6).
- [[⁽³⁾]]
- Four steam dryer support brackets that are located on the reactor vessel and spaced at 90° intervals were explicitly modeled (see Section 3.9).
- Most welds were replaced by node-to-node connections; interconnected parts share common nodes along the welds. In other locations the constraint equations between nodal degrees of freedom were introduced as described in Section 3.9.

3.4 Perforated Plate Model

The perforated plates were modeled as solid plates with adjusted elastic and dynamic properties. Properties of the perforated plates were assigned according to the type and size of perforation. Based on [8], for an equilateral square pattern with given hole size and spacing, the effective moduli of elasticity were found.

The adjusted properties for the perforated plates are shown in Table 2 as ratios to material properties of structural steel, provided in Table 1. Locations of perforated plates are classified by steam entry / exit vane bank side and vertical position.

Tests were carried out to verify that this representation of perforated plates by continuous ones with modified elastic properties preserves the modal properties of the structure. These tests are summarized in Appendix C of [6] and compare the predicted first modal frequency for a cantilevered perforated plate against an experimentally measured value. The prediction was obtained for a 40% open area plate (the maximum open area ratio of the perforated plates at BFN2, as seen in Table 2) using the analytical formula for a cantilevered plate and the modified Young's modulus and Poisson's ratio given by O'Donnell [8]. The measured and predicted frequencies are in close agreement, differing by less than 3%.

[[

(3)]]

[[

(3)]]

Figure 3. [[

(3)]]

Table 2. Material properties of perforated plates.

[[

(3)]]

3.5 Vane Bank Model

The vane bank assemblies consist of many vertical angled plates that are computationally expensive to model explicitly, since a prohibitive number of elements would be required. These parts have significant weight which is transmitted through the surrounding structure, so it is important to capture their gross inertial properties. Here the vane banks are modeled as a collection of point masses located at the center of mass for each vane bank section (Figure 4). The following masses were used for the vane bank sections, based on data found on provided drawings:

inner banks, 1575 lbm, 4 sections per bank;

middle banks, 1450 lbm, total 4 sections per bank; and
outer banks, 1515 lbm, 3 sections per bank.

These masses were applied to the base plates and vane top covers using the standard ANSYS point mass modeling option, element MASS21. ANSYS automatically distributes the point mass inertial loads to the nodes of the selected structure. The distribution algorithm minimizes the sum of the squares of the nodal inertial forces, while ensuring that the net forces and moments are conserved. Vane banks are not exposed to main steam lines directly, but rather shielded by the hoods.

The collective stiffness of the vane banks is expected to be small compared to the surrounding support structure and is neglected in the model. In the static case it is reasonable to expect that this constitutes a conservative approach, since neglecting the stiffness of the vane banks implies that the entire weight is transmitted through the adjacent vane bank walls and supports. In the dynamic case the vane banks exhibit only a weak response since (i) they have large inertia so that the characteristic acoustically-induced forces divided by the vane masses and inertias yield small amplitude motions, velocities and accelerations; and (ii) they are shielded from acoustic loads by the hoods, which transfer dynamic loads to the rest of the structure. Thus, compared to the hoods, less motion is anticipated on the vane banks so that approximating their inertial properties with equivalent point masses is justified. Nevertheless, the bounding parts, such as perforated plates, side panels, and top covers, are retained in the model. Errors associated with the point mass representation of the vane banks are compensated for by frequency shifting of the applied loads.

3.6 Water Inertia Effect on Submerged Panels

Water inertia was modeled by an increase in density of the submerged structure to account for the added hydrodynamic mass. This added mass was found by a separate hydrodynamic analysis (included in DRF-TVA-250B supporting this report) to be 0.1928 lbm/in² on the submerged skirt area. This is modeled by effectively increasing the material density for the submerged portions of the skirt. Since the skirt is 0.25 inches thick, the added mass is equivalent to a density increase of 0.771 lbm/in³. This added water mass was included in the ANSYS model by appropriately modifying the density of the submerged structural elements when computing harmonic response. For the static stresses, the unmodified density of steel is used throughout.

3.7 Structural Damping

Structural damping was defined as 1% of critical damping for all frequencies. This damping is consistent with guidance given on pg. 10 of NRC RG-1.20 [12].

3.8 Mesh Details and Element Types

Shell elements were employed to model the skirt, hoods, perforated plates, side and end plates, trough bottom plates, reinforcements, base plates and cover plates. Specifically, the four-node, Shell Element SHELL63, was selected to model these structural components. This element models bending and membrane stresses, but omits transverse shear. The use of shell elements is appropriate for most of the structure where the characteristic thickness is small compared to the other plate dimensions. For thicker structures, such as the upper and lower

support rings, solid brick elements were used to provide the full 3D stress. Tie bars were modeled with BEAM188 beam elements. The elements SURF154 are used to assure proper application of pressure loading to the structure. Mesh details and element types are shown in Table 3 and Table 4.

The mesh is generated automatically by ANSYS with refinement near edges. The maximum allowable mesh spacing is specified by the user. Here a 2.5 inch maximum allowable spacing is specified everywhere except in the following areas: drain pipes (1.5 inch maximum spacing); base plates (2 inches); tie rods (0.5 inches); and the curved portions of the drain channels (1 inch). Details of the finite element mesh are shown in Figure 5. Numerical experiments carried out using the ANSYS code applied to simple analytically tractable plate structures with dimensions and mesh spacings similar to the ones used for the steam dryer, confirm that the natural frequencies are accurately recovered (less than 1% errors for the first modes). These errors are compensated for by the use of frequency shifting.

3.9 Connections Between Structural Components

Most connections between parts are modeled as node-to-node connections. This is the correct manner (i.e., within the finite element framework) of joining elements away from discontinuities. At joints between shells, this approach omits the additional stiffness provided by the extra weld material. Also, locally 3D effects are more pronounced. The latter effect is accounted for using weld factors. The deviation in stiffness due to weld material is negligible, since weld dimensions are on the order of the shell thickness. The consequences upon modal frequencies and amplitude are, to first order, proportional to t/L where t is the thickness and L a characteristic shell length. The errors committed by ignoring additional weld stiffness are thus small and readily compensated for by performing frequency shifts.

When joining shell and solid elements, however, the problem arises of properly constraining the rotations, since shell element nodes contain both displacement and rotational degrees of freedom at every node whereas solid elements model only the translations. A node-to-node connection would effectively appear to the shell element as a simply supported, rather than (the correct) cantilevered restraint and significantly alter the dynamic response of the shell structure.

To address this problem, constraint equations are used to properly connect adjacent shell- and solid-element modeled structures. Basically, all such constraints express the deflection (and rotation for shell elements) of a node, \mathbf{R}_1 , on one structural component in terms of the deflections/rotations of the corresponding point, \mathbf{P}_2 , on the other connected component. Specifically, the element containing \mathbf{P}_2 is identified and the deformations at \mathbf{P}_2 determined by interpolation between the element nodes. The following types of shell-solid element connections are used in the steam dryer model including the following:

1. Connections of shell faces to solid faces (Figure 6a). While only displacement degrees of freedom are explicitly constrained, this approach also implicitly constrains the rotational degrees of freedom when multiple shell nodes on a sufficiently dense grid are connected to the same solid face.
2. Connections of shell edges to solids (e.g., connection of the bottom of closure plates with the upper ring). Since solid elements do not have rotational degrees of freedom, the

coupling approach consisted of having the shell penetrate into the solid by one shell thickness and then constraining both the embedded shell element nodes (inside the solid) and the ones located on the surface of the solid structure (see Figure 6b). Numerical tests involving simple structures showed that this approach and penetration depth reproduce both the deflections and stresses of the same structure modeled using only solid elements or ANSYS' bonded contact technology. Continuity of rotations and displacements is achieved.

The use of constraint conditions rather than the bonded contacts advocated by ANSYS for connecting independently meshed structural components confers better accuracy and useful numerical advantages to the structural analysis of the steam dryer including better conditioned and smaller matrices. The smaller size results from the fact that equations and degrees of freedom are eliminated rather than augmented (in Lagrange multiplier-based methods) by additional degrees of freedom. Also, the implementation of contact elements relies on the use of very high stiffness elements (in penalty function-based implementations) or results in indefinite matrices (Lagrange multiplier implementations) with poorer convergence behavior compared to positive definite matrices.

The upper support ring rests on four support blocks which resist vertical and lateral displacement. Because the contact region between the blocks and upper support ring is small, the ring is considered free to rotate about the radial axis. Specifically nodal constraints (zero relative displacement) are imposed over the contact area between the steam dryer upper support ring and the support blocks. Two nodes on each support block are fixed as indicated in Figure 7. One node is at the center of the support block surface facing the vessel and the other node is 0.5" offset inside the block towards the steam dryer, half way to the nearest upper support ring node. This arrangement approximates the nonlinear contact condition where the ring can tip about the block.

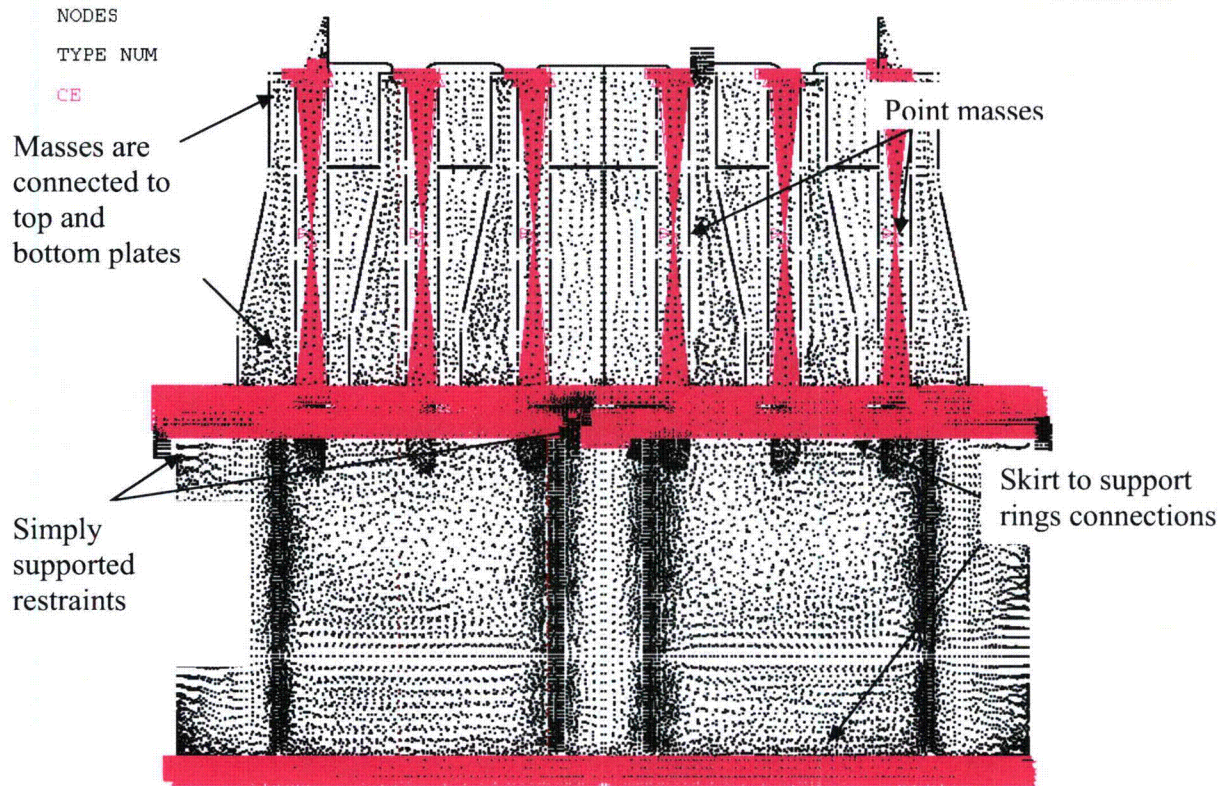


Figure 4. Point masses representing the vanes. The pink shading represents where constraint equations between nodes are applied.

Table 3. FE Model Summary.

Description	Quantity
Total Nodes ¹	133,564
Total Elements	115,085

1. Not including additional damper nodes and elements.

Table 4. Listing of Element Types.

Generic Element Type Name	Element Name	ANSYS Name
20-Node Quadratic Hexahedron	SOLID186	20-Node Hexahedral Structural Solid
10-Node Quadratic Tetrahedron	SOLID187	10-Node Tetrahedral Structural Solid
4-Node Elastic Shell	SHELL63	4-Node Elastic Shell
Mass Element	MASS21	Structural Mass
Pressure Surface Definition	SURF154	3D Structural Surface Effect
Beam element	BEAM188	3-D Finite Strain Beam
Damper element	COMBIN14	Spring-Damper

ANSYS10.0
WORKBENCH

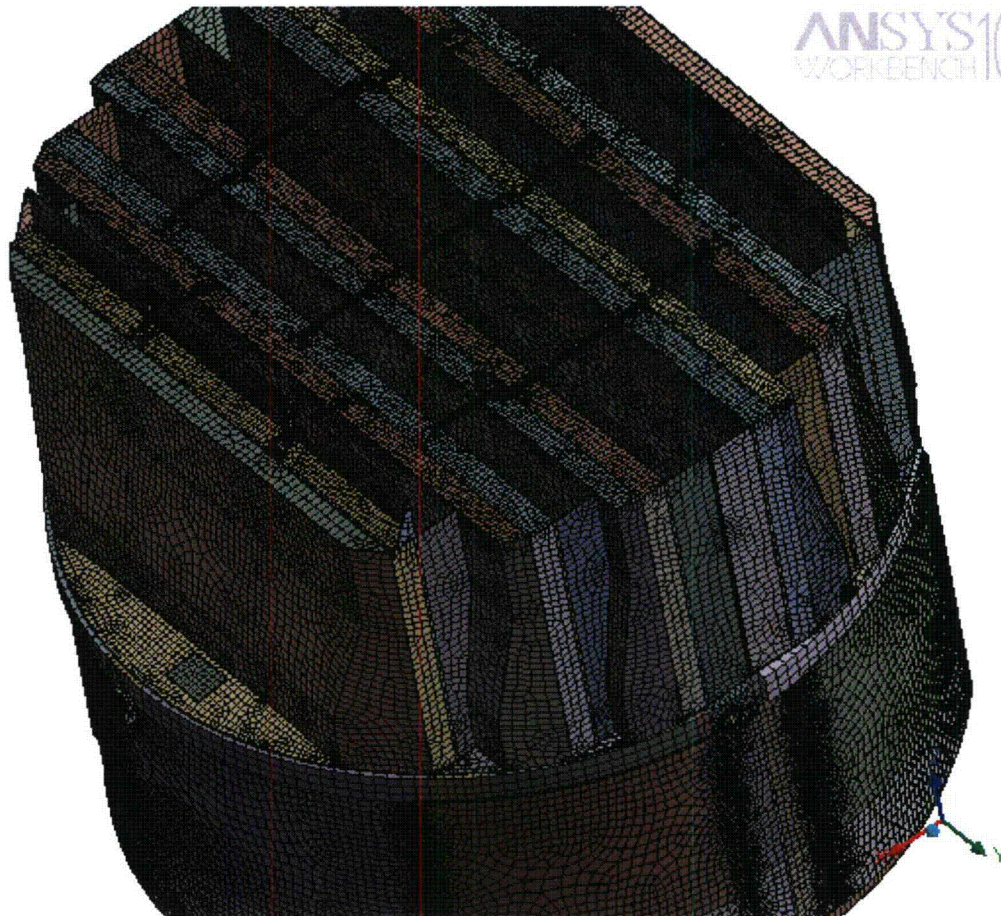


Figure 5a. Mesh overview.

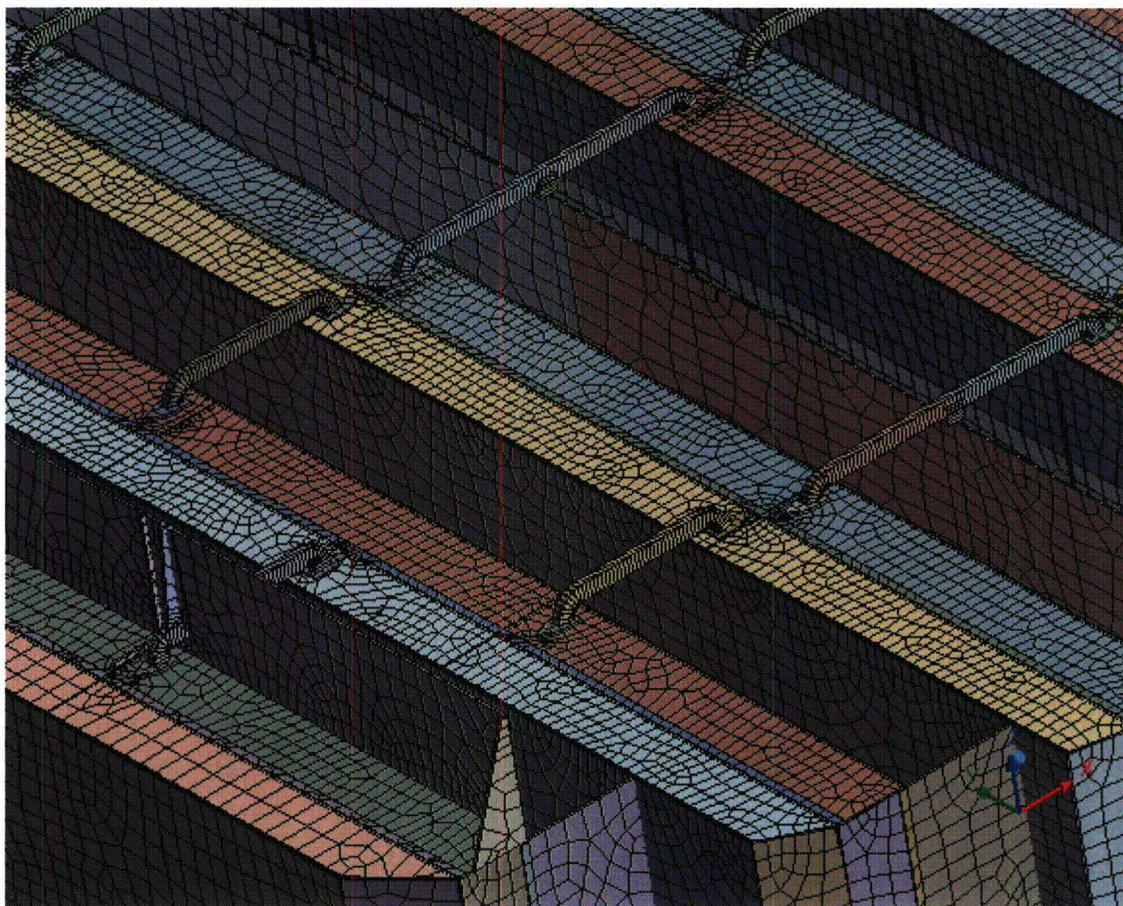


Figure 5b. Close up of mesh showing modified tie bars.



Figure 5c. Close up of mesh showing drain pipes and hood supports.

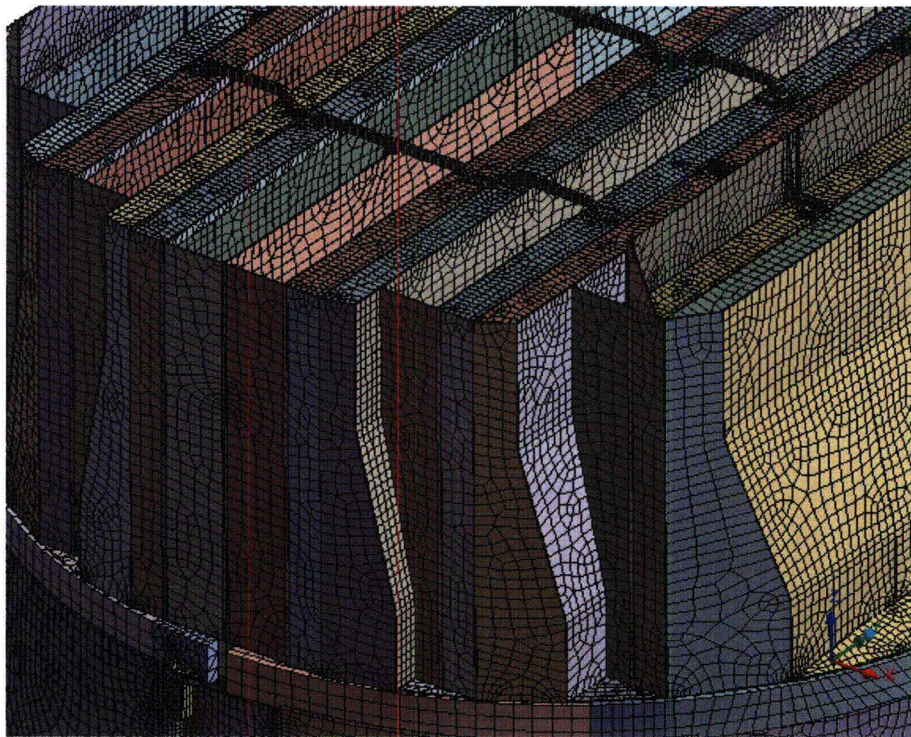


Figure 5d. Close up of mesh showing node-to-node connections between various plates.

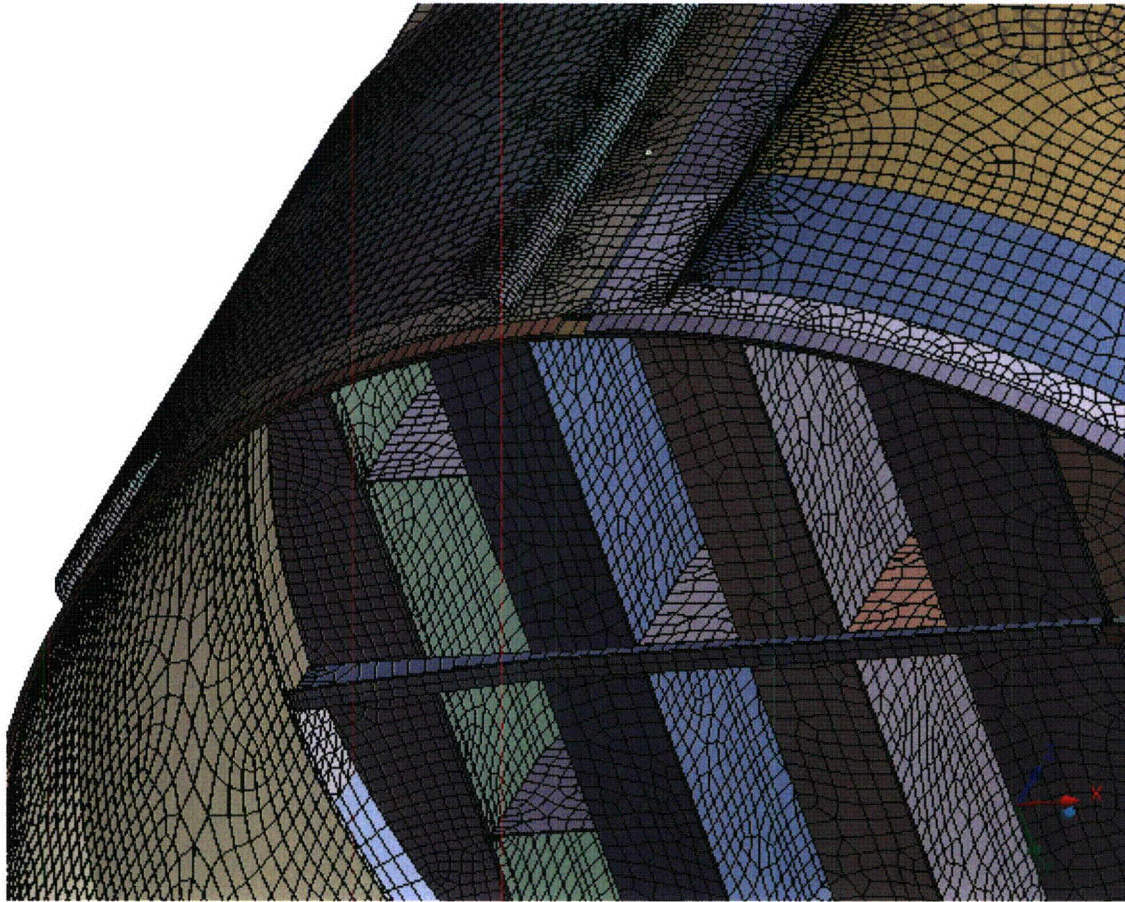


Figure 5e. Close up of mesh showing node-to-node connections between the skirt and drain channels; supporting beams and base plates; hood supports and hoods.



Figure 5f. Close up view of tie bars connecting vane cover plates and adjacent to the steam dam.

Shell nodes DOF are related to solid element shape functions

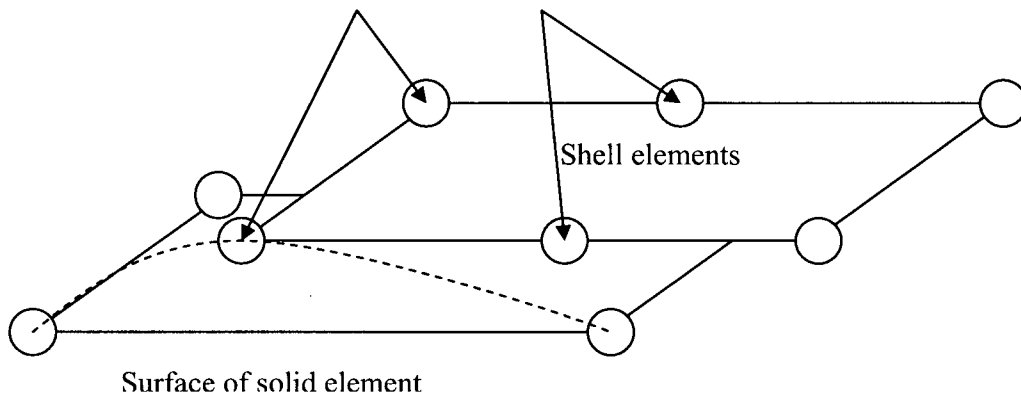


Figure 6a. Face-to-face shell to solid connection.

Shell nodes DOF are related to solid element shape functions

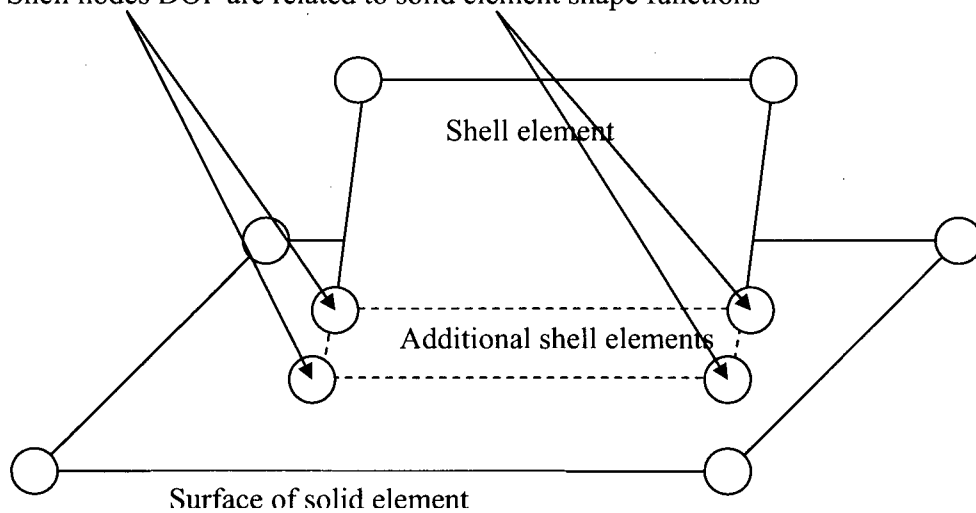


Figure 6b. Shell edge-to-solid face connection.

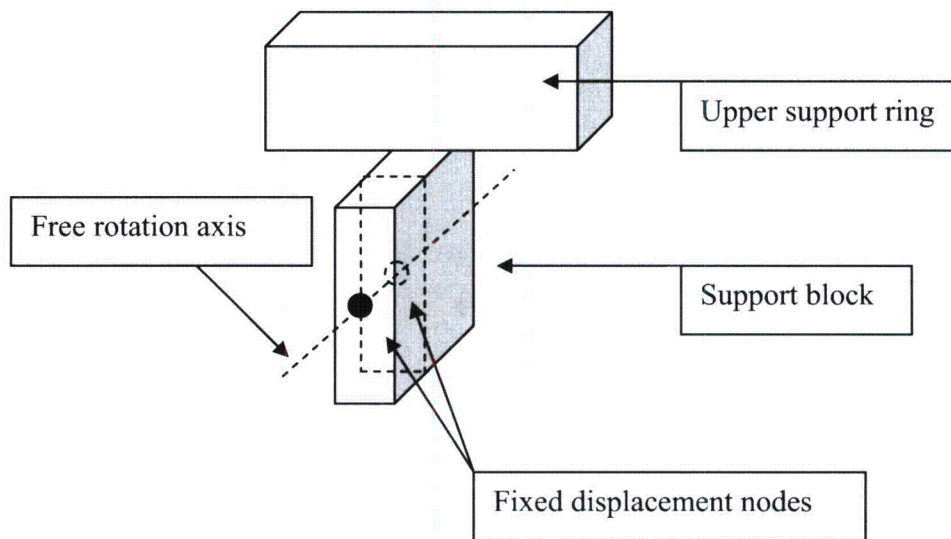


Figure 7. Boundary conditions. Inside node is half way between outer surface of support block and upper support ring.

3.10 Pressure Loading

The harmonic loads are produced by the pressures acting on the exposed surfaces of the steam dryer. At every frequency and for each MSL, the pressure distribution corresponding to a unit pressure at the MSL inlet is represented on a three-inch grid lattice grid (i.e., a mesh whose lines are aligned with the x-, y- and z-directions) that is superimposed over the steam dryer surface. This grid is compatible with the 'Table' format used by ANSYS to 'paint' general pressure distributions upon structural surfaces. The pressures are obtained from the Helmholtz solver routine in the acoustic analysis [1].

In general, the lattice nodes do not lie on the surface so that to obtain the pressure differences at the surface it is necessary to interpolate the pressure differences stored at the lattice nodes. This is done using simple linear interpolation between the 8 forming nodes of the lattice cell containing the surface point of interest. Inspection of the resulting pressures at selected nodes shows that these pressures vary in a well-behaved manner between the nodes with prescribed pressures. Graphical depictions of the resulting pressures and comparisons between the peak pressures in the original nodal histories and those in the final surface load distributions produced in ANSYS, all confirm that the load data are interpolated accurately and transferred correctly to ANSYS.

The harmonic pressure loads are only applied to surfaces above the water level, as indicated in Figure 8. In addition to the pressure load, the static loading induced by the weight of the steam dryer is analyzed separately. The resulting static and harmonic stresses are linearly combined to obtain total values which are then processed to calculate maximum and alternating stress intensities for assessment in Section 5.

[[

.⁽³⁾]] This is useful since revisions in the loads model do not necessitate recalculation of the unit stresses.

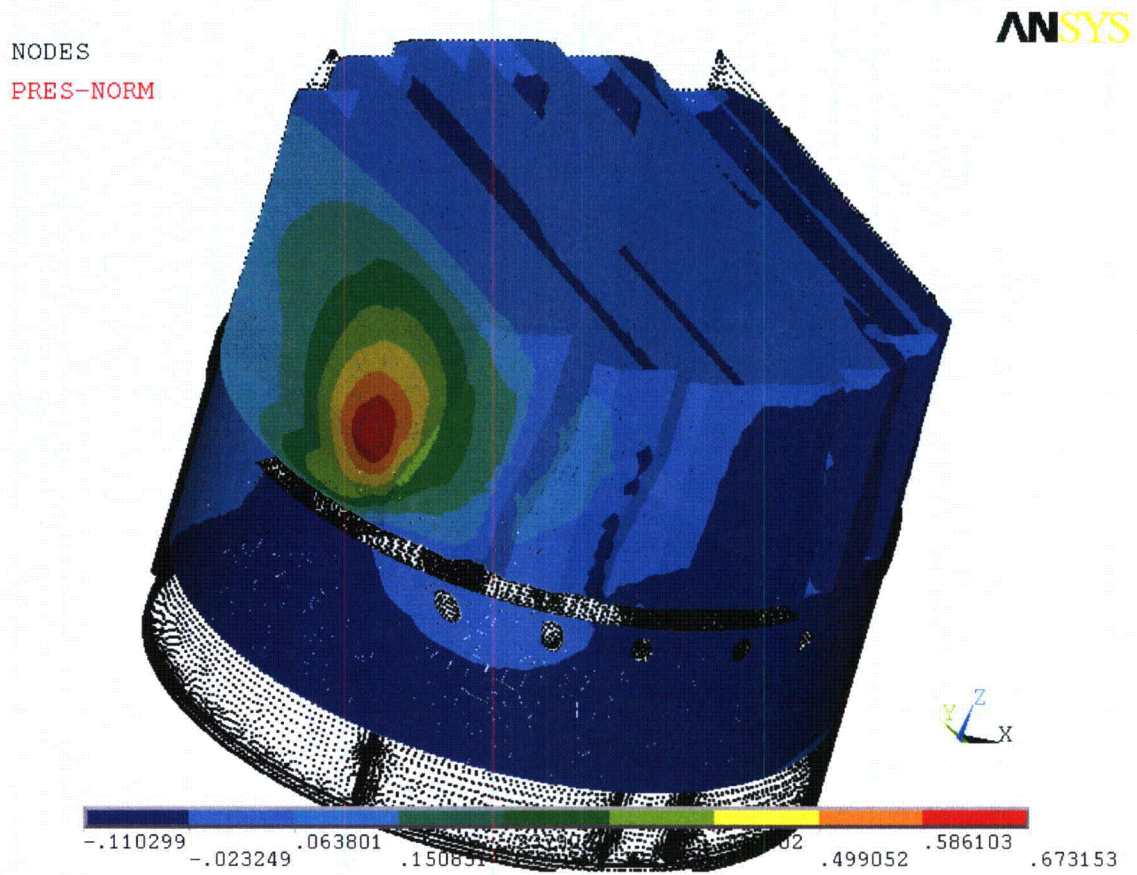


Figure 8a. Real part of unit pressure loading MSL C (in psid) on the steam dryer at 50.2 Hz. No loading is applied to the submerged transparent surface, solid support rings and dividing plates above the outer hoods.



NODES
PRES-NORM

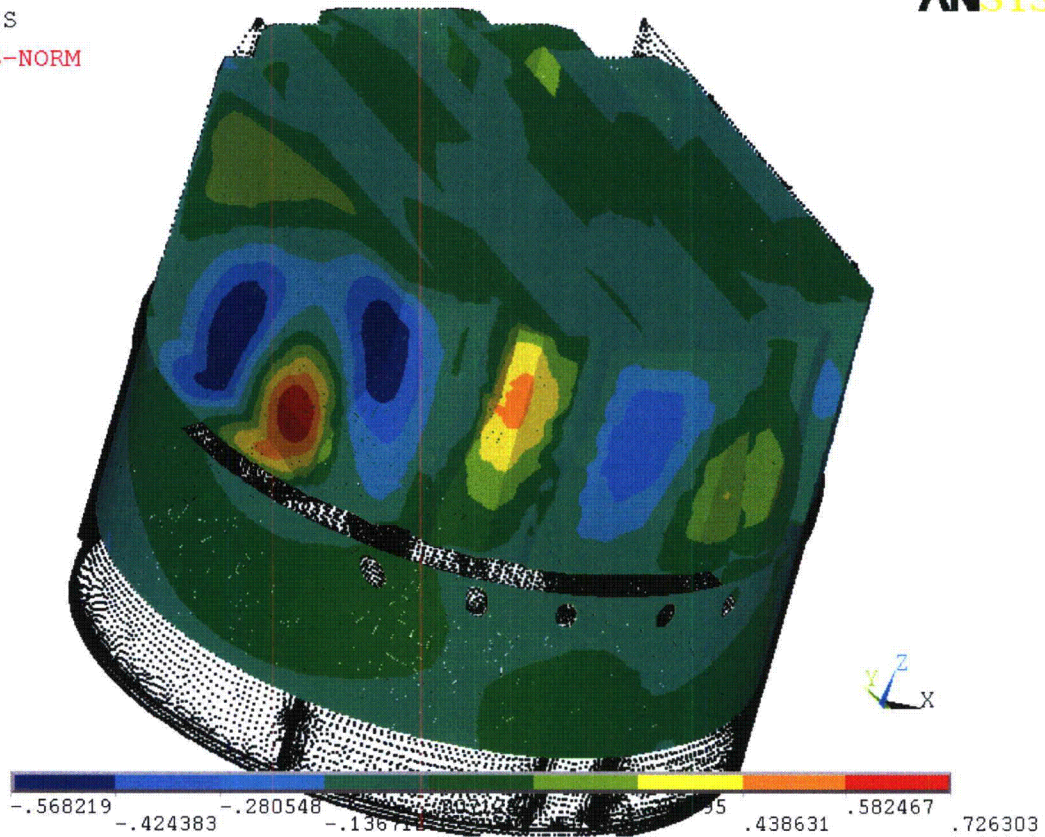


Figure 8b. Real part of unit pressure loading MSL C (in psid) on the steam dryer at 200.89 Hz. No loading is applied to the submerged transparent surface, solid support rings and dividing plates above the outer hoods.

4. Structural Analysis

The solution is decomposed into static and harmonic parts, where the static solution produces the stress field induced by the supported structure subjected to its own weight and the harmonic solution accounts for the harmonic stress field due to the unit pressure of given frequency in one of the main steam lines. All solutions are linearly combined, with amplitudes provided by signal measurements in each steam line, to obtain the final displacement and stress time histories. This decomposition facilitates the prescription of the added mass model accounting for hydrodynamic interaction and allows one to compare the stress contributions arising from static and harmonic loads separately. Proper evaluation of the maximum membrane and membrane+bending stresses requires that the static loads due to weight be accounted for. Hence both static and harmonic analyses are carried out.

4.1 Static Analysis

The results of the static analysis are shown in Figure 9. The locations with highest stress include the upper support ring areas near support brackets with stress intensity 5535 psi

4.2 Harmonic Analysis

The harmonic pressure loads were applied to the structural model at all surface nodes described in Section 3.10. Typical stress intensity distributions over the structure are shown in Figure 10. Stresses were calculated for each frequency, and results from static and harmonic calculations were combined.

To evaluate maximum stresses, the stress harmonics including the static component are transformed into a time history using FFT, and the maximum and alternating stress intensities for the response, evaluated. According to ASME B&PV Code, Section III, Subsection NG-3216.2 the following procedure was established to calculate alternating stresses. For every node, the stress difference tensors, $\sigma'_{nm} = \sigma_n - \sigma_m$, are considered for all possible pairs of the stresses σ_n and σ_m at different time levels, t_n and t_m . Note that all possible pairs require consideration since there are no "obvious" extrema in the stress responses. However, in order to contain computational cost, extensive screening of the pairs takes place (see Section 2.3) so that pairs known to produce alternating stress intensities less than 500 psi are rejected. For each remaining stress difference tensor, the principal stresses S_1, S_2, S_3 are computed and the maximum absolute value among principal stress differences, $S_{nm} = \max\{|S_1 - S_2|, |S_1 - S_3|, |S_2 - S_3|\}$, obtained. The alternating stress at the node is then one-half the maximum value of S_{nm} taken over all combinations (n,m), i.e., $S_{alt} = \frac{1}{2} \max_{n,m} \{S_{nm}\}$. This alternating stress is compared against allowable values, depending on the node location with respect to welds.



NODAL SOLUTION

STEP=1
SUB =1
TIME=1
USUM (AVG)
RSYS=0
DMX =.061518
SMX =.061518

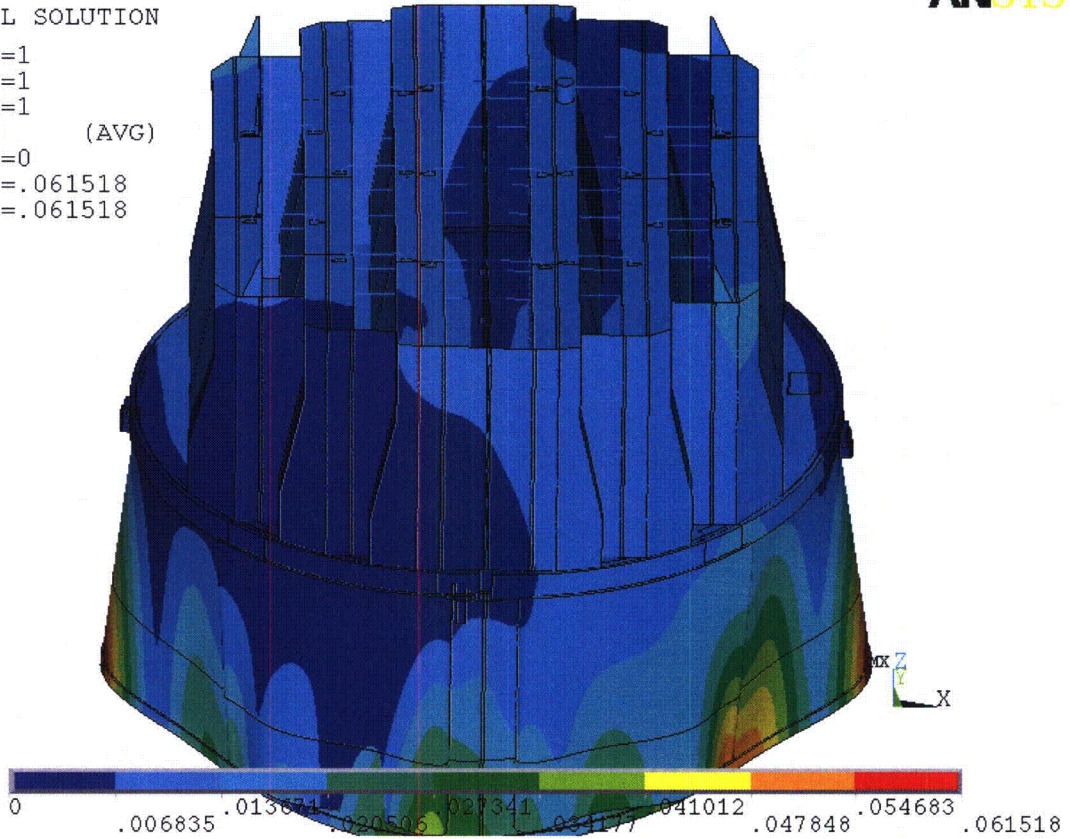


Figure 9a. Overview of static calculations showing displacements (in inches). Maximum displacement (DMX) is 0.05". Note that displacements are amplified for visualization.



NODAL SOLUTION

STEP=1
SUB =1
TIME=1
SINT (AVG)
DMX =.061518
SMN =.635523
SMX =5535

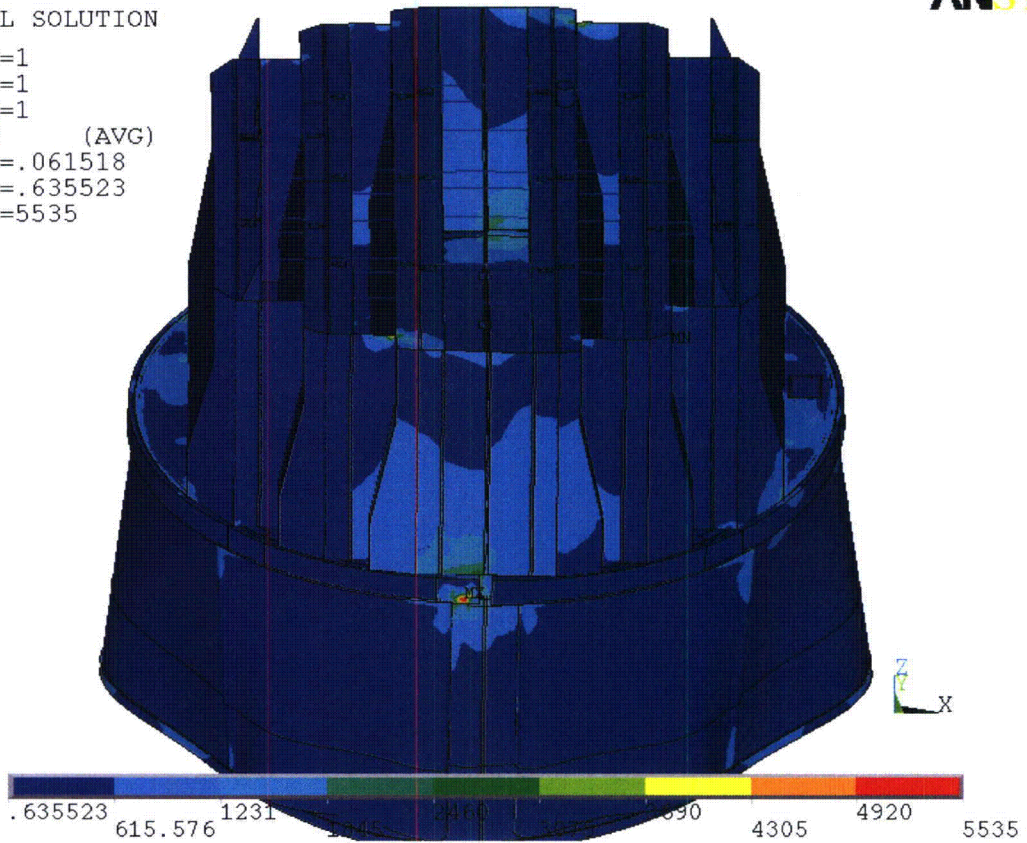


Figure 9b. Overview of static calculations showing stress intensities (in psi). Maximum stress intensity (SMX) is 5535 psi. Note that displacements are amplified for visualization



```
NODAL SOLUTION
STEP=1371
SUB =1
FREQ=50.207
REAL ONLY
SINT      (AVG)
DMX =.180434
SMN =.400388
SMX =9101
```

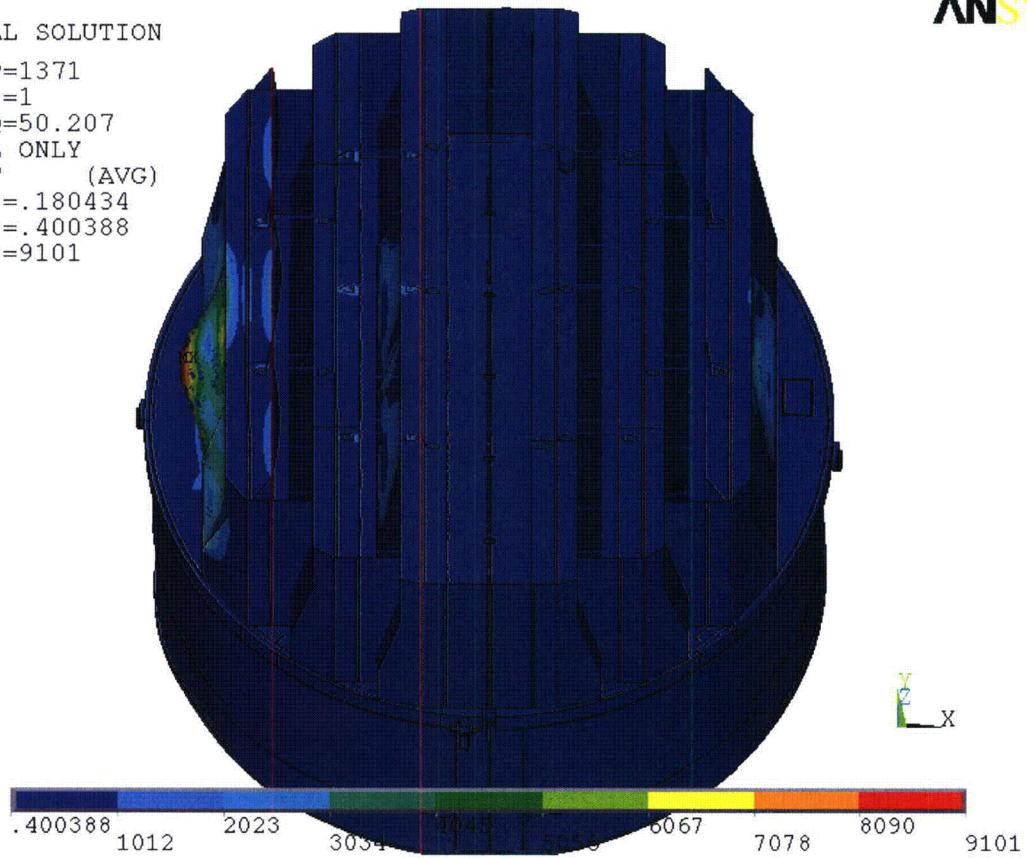


Figure 10a. Overview of harmonic calculations showing real part of stress intensities (in psi) along with displacements. Unit loading MSL C at 50.2 Hz (oriented to show high stress locations).



```
NODAL SOLUTION
STEP=275
SUB =1
FREQ=200.885
REAL ONLY
SINT (AVG)
DMX =.019771
SMN =.362065
SMX =8553
```

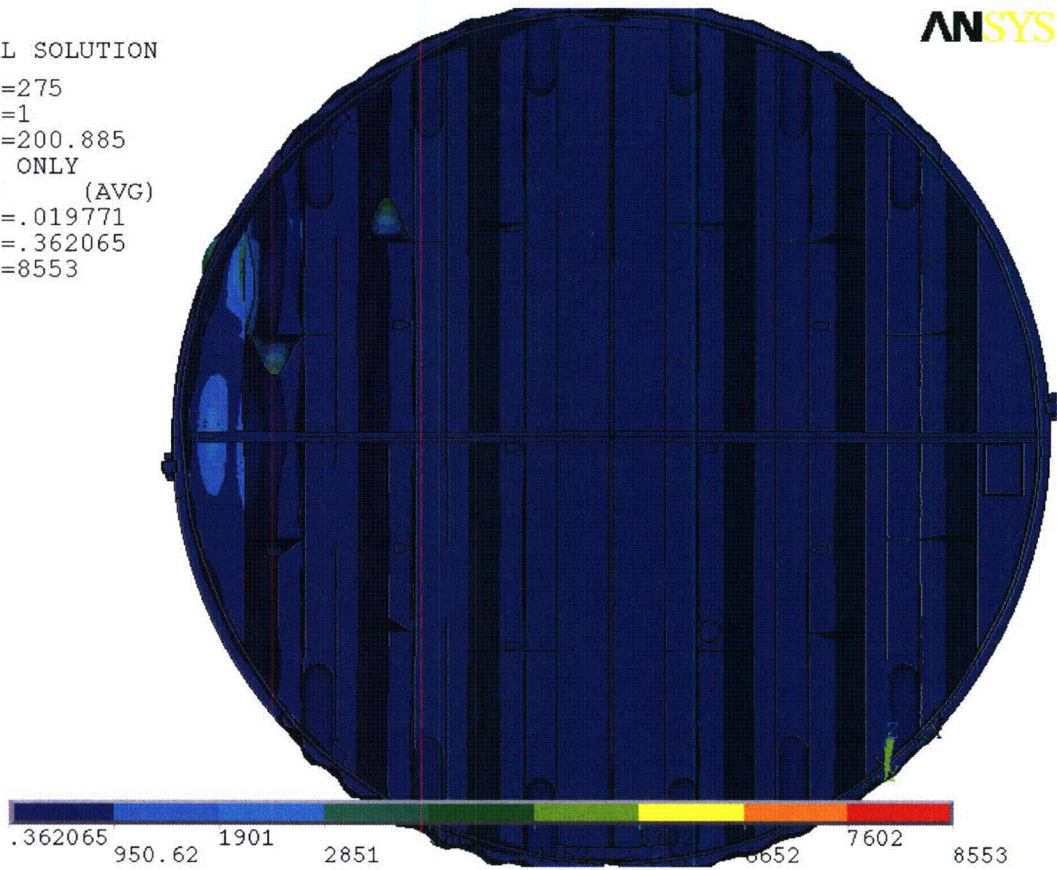


Figure 10b. Overview of harmonic calculations showing real part of stress intensities (in psi) along with displacements. Unit loading MSL C at 200.9 Hz (oriented to show high stress locations).

4.3 Post-Processing

The static and transient stresses computed at every node with ANSYS were exported into files for subsequent post-processing. These files were then read into separate customized software to compute the maximum and alternating stresses at every node. The maximum stress was defined for each node as the largest stress intensity occurring during the time history. Alternating stresses were calculated according to the ASME standard described above. For shell elements the maximum stresses were calculated separately at the mid-plane, where only membrane stress is present, and at top/bottom of the shell, where bending stresses are also present.

For nodes that are shared between several structural components or lie on junctions, the maximum and alternating stress intensities are calculated as follows. First, the nodal stress tensor is computed separately for each individual component by averaging over all finite elements meeting at the node and belonging to the same structural component. The time histories of these stress tensors are then processed to deduce the maximum and alternating stress intensities for each structural component. Finally for nodes shared across multiple components the highest of the component-wise maximum and alternating stresses is recorded as the "nodal" stress. This approach prevents averaging of stresses across components and thus yields conservative estimates for nodal stresses at the weld locations where several components are joined together.

The maximum stresses are compared against allowable values which depend upon the stress type (membrane, membrane+bending, alternating – P_m , P_m+P_b , S_{alt}) and location (at a weld or away from welds). These allowables are specified in the following section. For solid elements the most conservative allowable for membrane stress, P_m , is used, although bending stresses are nearly always present also. The structure is then assessed in terms of stress ratios formed by dividing allowables by the computed stresses at every node. Stress ratios less than unity imply that the associated maximum and/or alternating stress intensities exceed the allowable levels. Post-processing tools calculate the stress ratios, identifying the nodes with low stress ratios and generating files formatted for input to the 3D graphics program, TecPlot, which provides more general and sophisticated plotting options than currently available in ANSYS.

4.4 Computation of Stress Ratios for Structural Assessment

The ASME B&PV Code, Section III, subsection NG provides different allowable stresses for different load combinations and plant conditions. The stress levels of interest in this analysis are for the normal operating condition, which is the Level A service condition. The load combination for this condition is:

$$\text{Normal Operating Load Combination} = \text{Weight} + \text{Pressure} + \text{Thermal}$$

The weight and fluctuating pressure contributions have been calculated in this analysis and are included in the stress results. The static pressure differences and thermal expansion stresses are small, since the entire steam dryer is suspended inside the reactor vessel and all surfaces are exposed to the same conditions. Seismic loads only occur in Level B and C cases, and are not considered in this analysis.

Allowable Stress Intensities

The ASME B&PV Code, Section III, subsection NG shows the following (Table 5) for the maximum allowable stress intensity (S_m) and alternating stress intensity (S_a) for the Level A service condition. The allowable stress intensity values for type 304 stainless steel at operating temperature 550°F are taken from Table I-1.2 and Fig. I-9.2.2 of Appendix I of Section III, in the ASME B&PV Code. The calculation for different stress categories is performed in accordance with Fig. NG-3221-1 of Division I, Section III, subsection NG.

Table 5. Maximum Allowable Stress Intensity and Alternating Stress Intensity for all areas other than welds. The notation P_m represents membrane stress; P_b represents stress due to bending; Q represents secondary stresses (from thermal effects and gross structural discontinuities, for example); and F represents additional stress increments (due to local structural discontinuities, for example).

Type	Notation	Service Limit	Allowable Value (psi)
<i>Maximum Stress Allowables:</i>			
General Membrane	P_m	S_m	18,300
Membrane + Bending	$P_m + P_b$	$1.5 S_m$	27,450
Primary + Secondary	$P_m + P_b + Q$	$3.0 S_m$	54,900
<i>Alternating Stress Allowable:</i>			
Peak = Primary + Secondary + F	S_{alt}	S_a	13,600

When evaluating welds, either the calculated or allowable stress was adjusted, to account for stress concentration factor and weld quality. Specifically:

- For maximum allowable stress intensity, the allowable value is decreased by multiplying its value in Table 5 by 0.55.
- For alternating stress intensity, the calculated weld stress intensity is multiplied by a weld stress intensity (fatigue) factor of 1.8, before comparison to the S_a value given above.

The weld factors of 0.55 and 1.8 were selected based on the observable quality of the shop welds and liquid penetrant NDE testing of all welds (excluding tack and intermittent welds, which were subject to 5X visual inspection) during fabrication. These factors are consistent with fatigue strength reduction factors recommended by the Welding Research Council, [13], and stress concentration factors at welds, provided in [14] and [15]. In addition, critical welds are subject to periodical visual inspections in accordance with the requirements of GE SIL 644 SIL and BWR VIP-139 [16]. Therefore, for weld stress intensities, the allowable values are shown in Table 6.

These factors (0.55 and 1.8) also conservatively presume that the structure is joined using fillet welds unless specified otherwise. Since fillet welds correspond to larger stress concentration factors than other types of welds, this assumption is a conservative one.

Table 6. Weld Stress Intensities.

Type	Notation	Service Limit	Allowable Value (psi)
<i>Maximum Stress Allowables:</i>			
General Membrane	Pm	0.55 Sm	10,065
Membrane + Bending	Pm + Pb	0.825 Sm	15,098
Primary + Secondary	Pm + Pb + Q	1.65 Sm	30,195
<i>Alternating Stress Allowables:</i>			
Peak = Primary + Secondary + F	S _{alt}	Sa	13,600

Comparison of Calculated and Allowable Stress Intensities

The classification of stresses into general membrane or membrane + bending types was made according to the exact location, where the stress intensity was calculated; namely, general membrane, Pm, for middle surface of shell element, and membrane + bending, Pm + Pb, for other locations. For solid elements the most conservative, general membrane, Pm, allowable is used.

The structural assessment is carried out by computing stress ratios between the computed maximum and alternating stress intensities, and the allowable levels. Locations where any of the stresses exceed allowable levels will have stress ratios less than unity. Since computation of stress ratios and related quantities within ANSYS is time-consuming and awkward, a separate FORTRAN code was developed to compute the necessary maximum and alternating stress intensities, Pm, Pm+Pb, and S_{alt}, and then compare it to allowables. Specifically, the following quantities were computed at every node:

1. The maximum membrane stress intensity, Pm (evaluated at the mid-thickness location for shells),
2. The maximum membrane+bending stress intensity, Pm+Pb, (taken as the largest of the maximum stress intensity values at the bottom, top, and mid thickness locations, for shells),
3. The alternating stress, S_{alt}, (the maximum value over the three thickness locations is taken).
4. The stress ratio due to a maximum stress intensity assuming the node lies at a non-weld location (note that this is the minimum ratio obtained considering both membrane stresses and membrane+bending stresses):

$$SR-P(nw) = \min \{ Sm/Pm, 1.5 * Sm/(Pm+Pb) \}.$$
5. The alternating stress ratio assuming the node lies at a non-weld location,

$$SR-a(nw) = Sa / (1.1 * S_{alt}),$$
6. The same as 4, but assuming the node lies on a weld,

$$SR-P(w) = SR-P(nw) * f_{sw} * 0.55$$
7. The same as 5, but assuming the node lies on a weld,

$$SR-a(w) = SR-a(nw) * f_{sw} / 1.8.$$

where $f_{sw}=1$ at all welds (when justified, f_{sw} can be adjusted to reflect different weld types). Note that in steps 4 and 6, the minimum of the stress ratios based on P_m and P_m+P_b , is taken. The allowables listed in Table 6, $S_m=18,300$ psi and $S_a=13,600$ psi. The factors, 0.55 and 1.8, are the weld factors discussed above. The factor of 1.1 accounts for the differences in Young's moduli for the steel used in the steam dryer and the values assumed in alternating stress allowable. According to NG-3222.4 in subsection NG of Section III of the ASME Code, the effect of elastic modulus upon alternating stresses is taken into account by multiplying alternating stress S_{alt} at all locations by the ratio, $E/E_{model}=1.1$, where:

$$E = 28.3 \cdot 10^6 \text{ psi, as shown on Fig. I-9.2.2. ASME BP\&V Code}$$
$$E_{model} = 25.55 \cdot 10^6 \text{ psi (Table 1)}$$

The nodes with stress ratios lower than 4 are plotted in TecPlot (a 3D graphics plotting program widely used in engineering communities [17]) to establish whether they lie on a weld or not. The appropriate maximum and alternating stress ratios, SR-P and SR-a, are thus determined and a final listing of nodes having the smallest stress ratios is generated. These nodes are tabulated and depicted in the Results Sections.

5. Results

The stress intensities and associated stress ratios resulting from the Rev. 4 acoustic/hydrodynamic loads [2] with associated biases and uncertainties factored in, are presented below. The bias due to finite frequency discretization and uncertainty associated with the finite element model itself, are also factored in. In the following sections the highest maximum and alternating stress intensities are presented to indicate which points on the dryer experience significant stress concentration and/or modal response (Section 5.1). The lowest stress ratios obtained by comparing the stresses against allowable values, accounting for stress type (maximum and alternating) and location (on or away from a weld), are also reported (Section 5.2). Finally the frequency dependence of the stresses at nodes experiencing the lowest stress ratios is depicted in the form of accumulative PSDs (Section 5.3).

In each section results are presented both at nominal conditions (no frequency shift) and with frequency shift included. Unless specified otherwise, frequency shifts are generally performed at 2.5% increments. The tabulated stresses and stress ratios are obtained using a 'blanking' procedure that is designed to prevent reporting a large number of high stress nodes from essentially the same location on the structure. In the case of stress intensities this procedure is as follows. The relevant stress intensities are first computed at every node and then nodes sorted according to stress level. The highest stress node is noted and all neighboring nodes within 10 inches of the highest stress node and its symmetric images (i.e., reflections across the $x=0$ and $y=0$ planes) are "blanked" (i.e., excluded from the search for subsequent high stress locations). Of the remaining nodes, the next highest stress node is identified and its neighbors (closer than 10 inches) blanked. The third highest stress node is similarly located and the search continued in this fashion until all nodes are either blanked or have stresses less than half the highest value on the structure. For stress ratios, an analogous blanking procedure is applied. Thus the lowest stress ratio of a particular type in a 10" neighborhood and its symmetric images is identified and all other nodes in these regions excluded from listing in the table. Of the remaining nodes, the one with the lowest stress ratio is reported and its neighboring points similarly excluded, and so on until all nodes are either blanked or have a stress ratio higher than 4.

The measured CLTP strain gage signals contain significant contributions from non-acoustic sources such as sensor noise, MSL turbulence and pipe bending vibration that contribute to the hoop strain measurements. The ACM analysis does not distinguish between the acoustic and non-acoustic fluctuations in the MSL signals that could lead to sizeable, but fictitious acoustic loads and resulting stresses on the dryer. One way to remove these fictitious loads is to collect data with the system maintained at operating pressure (1000 psi) and temperature, but low (less than 20% of CLTP) flow. By operating the recirculation pumps at this condition, the background plant noise and vibrations remain present. At these conditions the acoustic loads are known to be negligible so that collected data, referred to as the 1000 psig data, originate entirely from non-acoustic sources such as sensor noise and mechanical vibrations. This information is valuable since it allows one to now distinguish between the acoustic and non-acoustic content in the CLTP signal and therefore modify the CLTP loads so that only the acoustic component is retained. For consistency, the 1000 psig strain gage signals are filtered in the same manner as the CLTP data and are fed into the ACM model to obtain the monopole and dipole signals at the MSL inlets. Since there is negligible flow, these signals are fictitious, i.e., the hoop strains

measured by the strain gages are not due to pressure fluctuations, but rather due to noise. However, under the supposition that these signals are acoustic in origin the hypothetical stresses due to these signals can nevertheless be computed.

The contribution of background noise in the Browns Ferry Unit 2 steam dryer was quantified by taking strain gage measurements at 19% power. At this level there are no significant acoustic sources. To compensate for the non-acoustic noise source represented in the 1000 psig data, the CLTP MSL inlet pressure signals are modified according to:

$$P(f) = P_0(f) * \max \left[0, 1 - \frac{\bar{N}(f)}{\bar{P}_0(f)} \right] \quad (8)$$

where f is the frequency (in Hz), $P_0(f)$ is the MSL inlet pressure (monopole or dipole) at CLTP conditions before correction, $P(f)$ is the corresponding post-correction pressure and $\bar{N}(f)$ and $\bar{P}_0(f)$ are averaged pressure amplitudes associated with the 1000 psig data and CLTP data respectively. Specifically,

$$\bar{P}_0(f) = \frac{1}{2} \int_{f-1}^{f+1} |P_0(f)| df \quad (9)$$

where $|P_0(f)|$ denotes the absolute value of the complex quantity. Hence $\bar{P}_0(f)$ is the average amplitude of the CLTP pressure in the ± 1 Hz interval about frequency, f . The same definition, but using the 1000 psig pressure signal, is used for $\bar{N}(f)$. Note that this modification leaves the phase information in the original CLTP signal unchanged.

The applied load includes all biases and uncertainties for both the ACM (summarized in [2]) and the FEM. For the latter there are three main contributors to the bias and uncertainty. The first is an uncertainty (25.26%) that accounts for modeling idealizations (e.g., vane bank mass model), geometrical approximations and other discrepancies between the modeled and actual dryer such as neglecting of weld mass and stiffness in the FEA. The second contributor is a bias (5.72%) accounting for discretization errors associated with using a finite size mesh, upon computed stresses. The third contributor is also a bias and compensates for the use of a finite discretization schedule in the construction of the unit solutions. The frequencies are spaced such that at 1% damping the maximum (worst case) error in a resonance peak is 5%. The average error for this frequency schedule is 1.72%.

5.1 General Stress Distribution and High Stress Locations

The maximum stress intensities obtained by post-processing the ANSYS stress histories for CLTP at nominal frequency and with frequency shift operating conditions are listed in Table 7. Contour plots of the stress intensities over the steam dryer structure are shown on Figure 11 (nominal frequency) and Figure 12 (max. stress over all nine frequency shifts including nominal). The figures are oriented to emphasize the high stress regions. Note that these stress intensities *do not* account for weld factors but include end-to-end bias and uncertainty. Further,

it should be noted that since the allowable stresses vary with location, stress intensities do not necessarily correspond to regions of primary structural concern. Instead, structural evaluation is more accurately made in terms of the stress ratios which compare the computed stresses to allowable levels with due account made for stress type and weld factors. Comparisons on the basis of stress ratios are made in Section 5.2.

The maximum stress intensities in most areas are low (less than 500 psi). For the membrane stresses (P_m) the high stress regions tend to occur at: (i) the restraint locations for the upper support ring; (ii) the upper edges of the closure plates and (iii) junctions connecting the bottoms of the hood supports. The first location experiences high stresses since the entire weight of the structure is transmitted through relatively small pads to the external structure. The stress is dominated by the static component since the stress intensities at this location do not vary significantly with frequency shift and alternating stress intensities remain below 1600psi at all shifts (see first row in Table 7b). The closure plates experience high stresses since they restrain displacements in the adjacent vane banks. The junctions where the hoods, hood supports and base or cover plates meet also experience high stresses.

The membrane + bending stress (P_m+P_b) distributions evidence a more distinguished modal response especially on the outer hoods. The first three regions showing high stress intensities are the same as for membrane stresses. (Note that for the first two nodes, 118466 and 118711, $P_m=P_m+P_b$ because these stresses occur in solid elements for which no distinction between membrane and bending stresses is made.) In addition stress concentrations are now more pronounced on welds where the outer hoods and underlying hood supports meet, especially near the bottom where these welds meet the cover plate as seen in Figure 12b and c. Stress concentrations are also observed on: (i) the tie bar bases (ii) the closure plates where they connect to the hoods or vane bank end plates; and (iii) the skirt/drain channel welds.

The alternating stress, S_{alt} , distributions are more localized, high values being obtained on the outer hoods and tie bar bases. The contour plots with and without frequency shifts are similar. When all frequency shifts are considered (Figure 12d) there is a stronger response on the outer hood end plates; also a weak modal response along the periphery of the submerged lower skirt is evident. The alternating response on the lock/lock gusset is believed artificially high because the gusset is modeled as connected to the tie bar. In reality the gusset rests on the tie bar and is in contact with it, but not connected so that the connection condition is nonlinear (the connection supports compressive stresses, but not tensile or shear stresses).

Comparing the nominal results (Table 7a) and results with frequency shifting it can be seen that maximum stress intensities, P_m and P_m+P_b , do not differ significantly. The alternating stresses however, are approximately 40% higher when frequency shifts are considered. Moreover, all nodes alternating stress intensity nodes listed in Table 7b assume their highest values at the +10% shift. As shown in the next section, all stresses are well within allowable levels.

Finally, the maximum stress intensities at any frequency shift for the locations in Table 7b are recomputed using the CLTP loads without noise removal and reported in Table 7c. These results show that the changes in stress intensities are generally small (10% or less).

Table 7a. Locations with highest predicted stress intensities for CLTP conditions with no frequency shift. Signal noise has been removed using 19% power data.

Stress Category	Location	Weld	Location (in)			node	Stress Intensities (psi)		
			x	y	z		Pm	Pm+Pb	S _{alt}
Pm	Upper Support Ring (USR)/Seismic Block/Support Block	No	-122.1	10	-9.5	118466	6813	6813	1460
"	USR part/Support Block/Support	No	7	122.3	-9.5	118711	6621	6621	1370
"	Top Cover Inner Hood/Middle Closure Plate/Inner Hood	Yes	31.5	108.4	88.9	96687	5539	6117	876
"	Outer Hood	No	102	-61.1	-0.1	43493	5280	5786	910
"	Splice Bar/USR part	Yes	2.2	119	0	118662	5198	5198	<500
Pm+Pb	USR/Seismic Block/Support Block	No	-122.1	10	-9.5	118466	6813	6813	1460
"	USR part/Support Block/Support	No	7	122.3	-9.5	118711	6621	6621	1370
"	Top Cover Inner Hood/Middle Closure Plate/Inner Hood	Yes	-31.5	-108.4	88.9	98968	5295	6134	801
"	Outer Hood	No	102	-61.1	-0.1	43493	5280	5786	910
"	Submerged Drain Channel/Skirt	Yes	-91	76.7	-100.5	89515	996	5432	1513
S _{alt}	Lock/Lock Gusset	No	-77	31.4	91.9	93557	2120	4872	3007
"	Top Cover/Top Tie Bar Base	Yes	-48	3	88.9	92532	390	3385	2925
"	Top Cover Inner Hood/Top Perf. Plate/Top Cover Overlap	Yes	-24	2.8	88.9	90207	604	2394	2366
"	Top Cover/Top Tie Bar Base	Yes	-48	-58.6	88.9	97521	226	2634	2240
"	Outer Side Panel/Vane Bank Thin/Vane Bank Thick/Outer End Wall	Yes	86	85	12.1	101181	487	2343	2015

Node numbers are retained for further reference.

Spatial coordinates are in a reference frame whose origin is located at the intersection of the steam dryer centerline and the plane containing the base and cover plates (this plane also contains the top of the upper support ring and the bottom edges of the hoods). The y-axis is parallel to the hoods, the x-axis is normal to the hoods pointing from MSL C/D to MSL A/B, and the z-axis is vertical, positive up.

Table 7b. Locations with highest predicted stress intensities taken over all frequency shifts CLTP conditions. Signal noise has been removed using 19% power data.

Stress Category	Location	Weld	Location (in)				Stress Intensities (psi)			% Freq. Shift
			x	y	z	node	Pm	Pm+Pb	S _{alt}	
Pm	USR part/Support Block/Support	No	7	122.3	-9.5	118711	6865	6865	1571	-10
"	USR/Seismic Block/Support Block	No	-122.1	10	-9.5	118466	6813	6813	1460	0
"	Top Cover Inner Hood/Middle Closure Plate/Inner Hood	Yes	31.5	108.4	88.9	96687	5735	6337	1090	+2.5
"	Outer Hood	No	102	-61.1	-0.1	43493	5361	5995	1183	+10
"	Splice Bar/USR part	Yes	2.2	119	0	118662	5359	5359	656	+10
Pm+Pb	USR part/Support Block/Support	No	7	122.3	-9.5	118711	6865	6865	1571	-10
"	USR/Seismic Block/Support Block	No	-122.1	10	-9.5	118466	6813	6813	1460	0
"	Top Cover Inner Hood/Middle Closure Plate/Inner Hood	Yes	-31.5	-108.4	88.9	98968	5585	6508	1080	+10
"	Lock/Lock Gusset	No	-77	31.4	91.9	93557	2505	6121	4104	+10
"	Outer Hood	No	102	-61.1	-0.1	43493	5361	5995	1183	+10
Salt	Top Cover/Top Tie Bar Base	Yes	48	3	88.9	96745	396	4582	4163	+10
"	Lock/Lock Gusset	No	-77	31.4	91.9	93557	2505	6121	4104	+10
"	Top Cover Inner Hood/Top Cover Overlap/Top Perf. Plate	Yes	24	2.8	88.9	88313	704	3812	3693	+10
"	Top Cover/Top Tie Bar Base	Yes	48	-58.6	88.9	97260	355	4147	3462	+10
"	Top Cover Inner Hood/Hood Support/Top Tie Bar Base	Yes	28.2	-59.9	88.9	100330	689	3402	2816	+10

See Table 7a for coordinates description.

Table 7c. Highest stress intensities at any frequency shift for the nodes listed in Table 7b computed using the unfiltered CLTP loads (i.e., signal noise has *not* been removed).

Stress Category	Location	Weld	Location (in)			node	Stress Intensities (psi)			% Freq. Shift
			x	y	z		Pm	Pm+Pb	S _{alt}	
Pm	USR part/Support Block/Support	No	7	122.3	-9.5	118711	6859	6859	1583	-10
"	USR/Seismic Block/Support Block	No	-122.1	10	-9.5	118466	6952	6952	1560	0
"	Top Cover Inner Hood/Middle Closure Plate/Inner Hood	Yes	31.5	108.4	88.9	96687	5930	6538	1246	+10
"	Outer Hood	No	102	-61.1	-0.1	43493	5631	6531	1815	+10
"	Splice Bar/USR part	Yes	2.2	119	0	118662	5377	5377	664	+10
Pm+Pb	USR part/Support Block/Support	No	7	122.3	-9.5	118711	6859	6859	1583	-10
"	USR/Seismic Block/Support Block	No	-122.1	10	-9.5	118466	6952	6952	1560	0
"	Top Cover Inner Hood/Middle Closure Plate/Inner Hood	Yes	-31.5	-108.4	88.9	98968	5814	6769	1268	+10
"	Lock/Lock Gusset	No	-77	31.4	91.9	93557	2991	6200	4399	+10
"	Outer Hood	No	102	-61.1	-0.1	43493	5594	6613	1828	+7.5
S _{alt}	Top Cover/Top Tie Bar Base	Yes	48	3	88.9	96745	514	4678	4315	+10
"	Lock/Lock Gusset	No	-77	31.4	91.9	93557	2991	6200	4399	+10
"	Top Cover Inner Hood/Top Cover Overlap/Top Perf. Plate	Yes	24	2.8	88.9	88313	727	3878	3786	+10
"	Top Cover/Top Tie Bar Base	Yes	48	-58.6	88.9	97260	497	4252	3578	+10
"	Top Cover Inner Hood/Hood Support/Top Tie Bar Base	Yes	28.2	-59.9	88.9	100330	919	3467	2881	+10

See Table 7a for coordinates description.

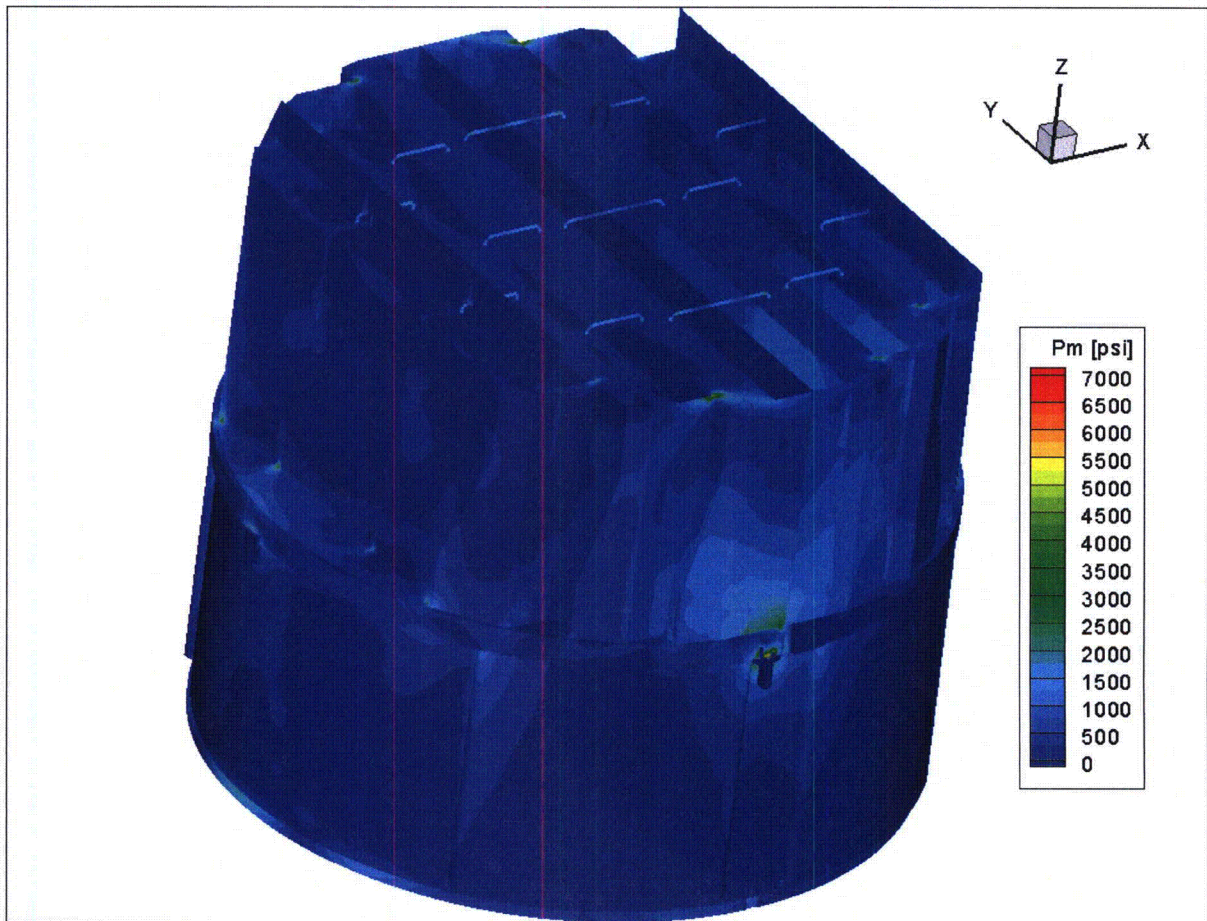


Figure 11a. Contour plot of maximum membrane stress intensity, P_m , for CLTP load. The maximum stress intensity is 6,813 psi.

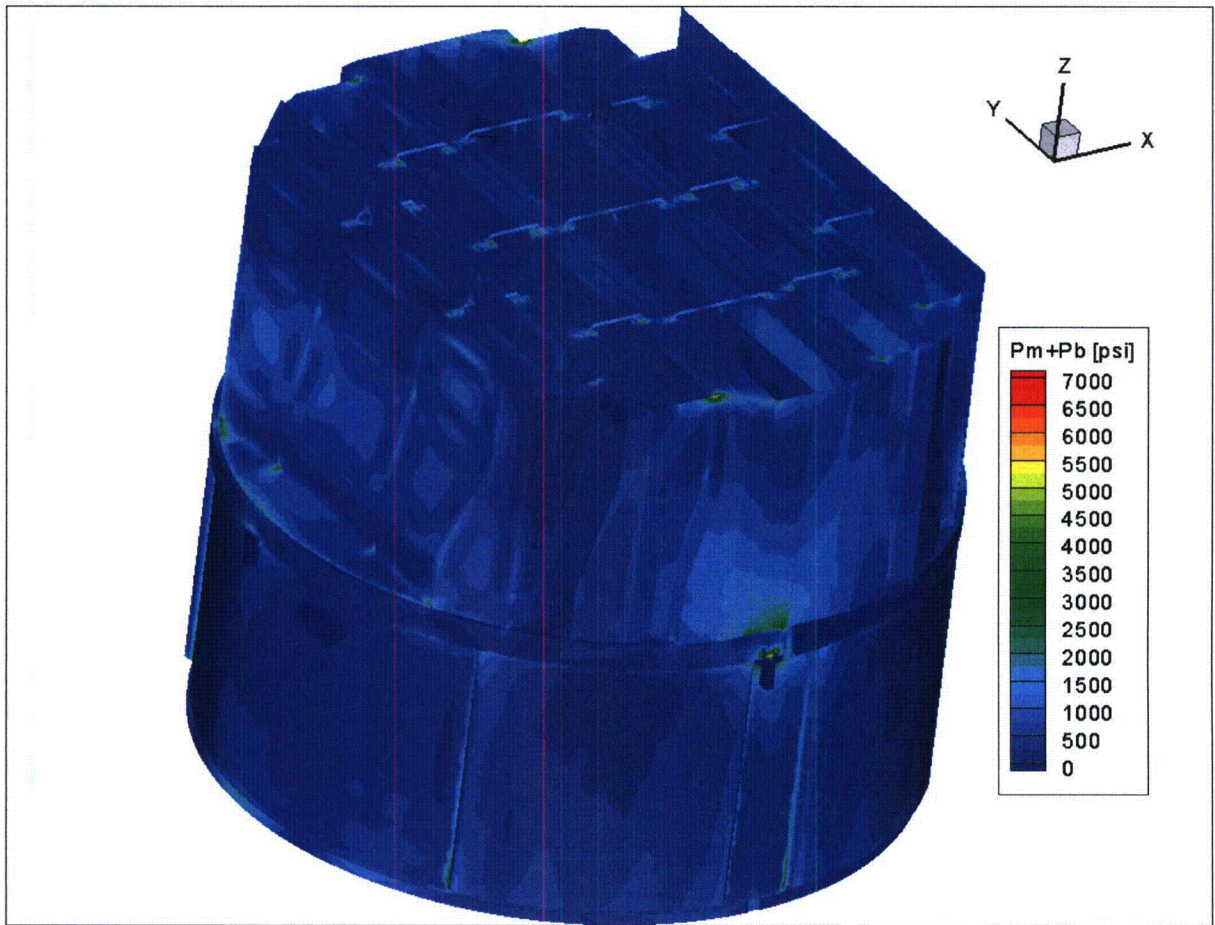


Figure 11b. Contour plot of maximum membrane+bending stress intensity, P_m+P_b , for CLTP load. The maximum stress intensity is 6,813 psi. First view.

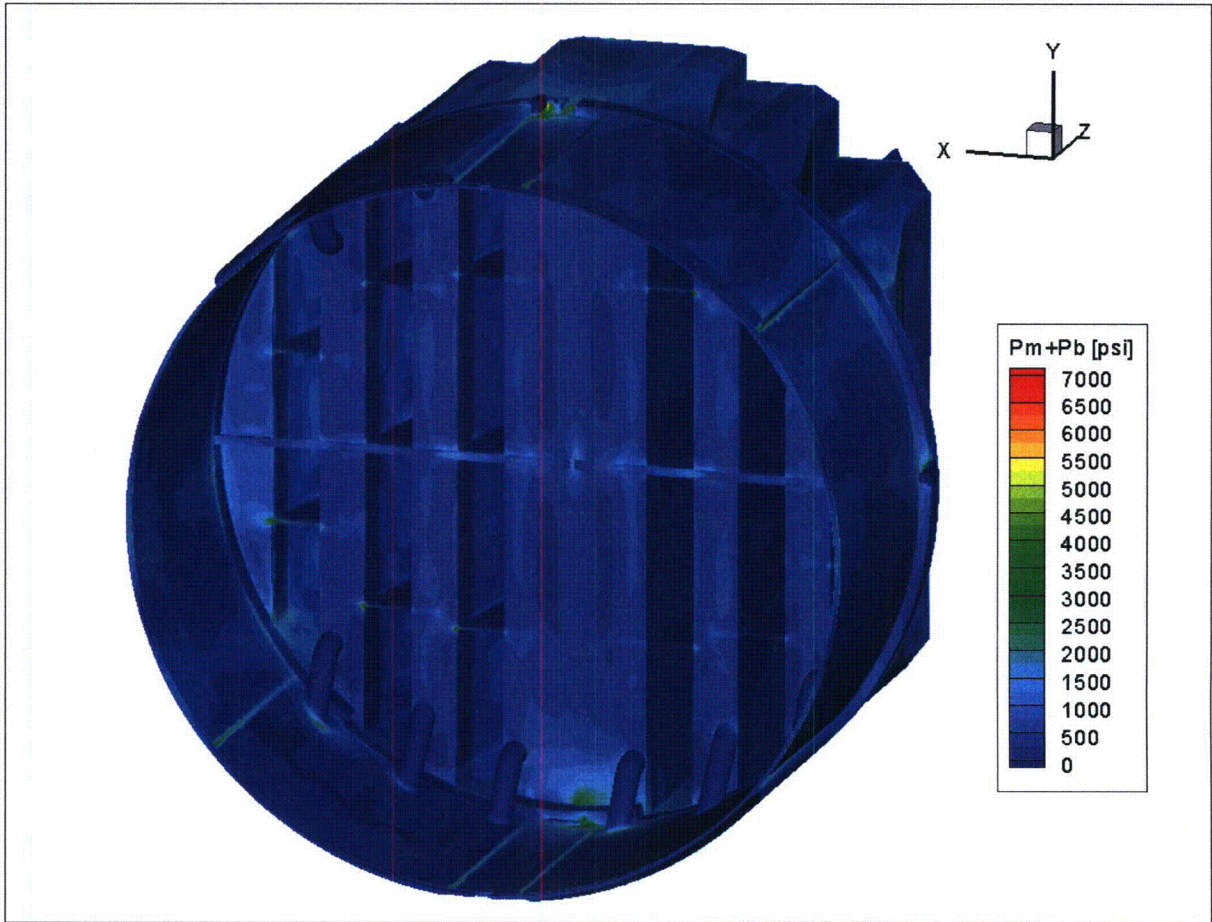


Figure 11c. Contour plot of maximum membrane+bending stress intensity, $P_m + P_b$, for CLTP load. This second view from below shows the high stress intensities at the bottom of the outer and middle hood supports, support beam, central base plates and drain pipe/skirt welds.

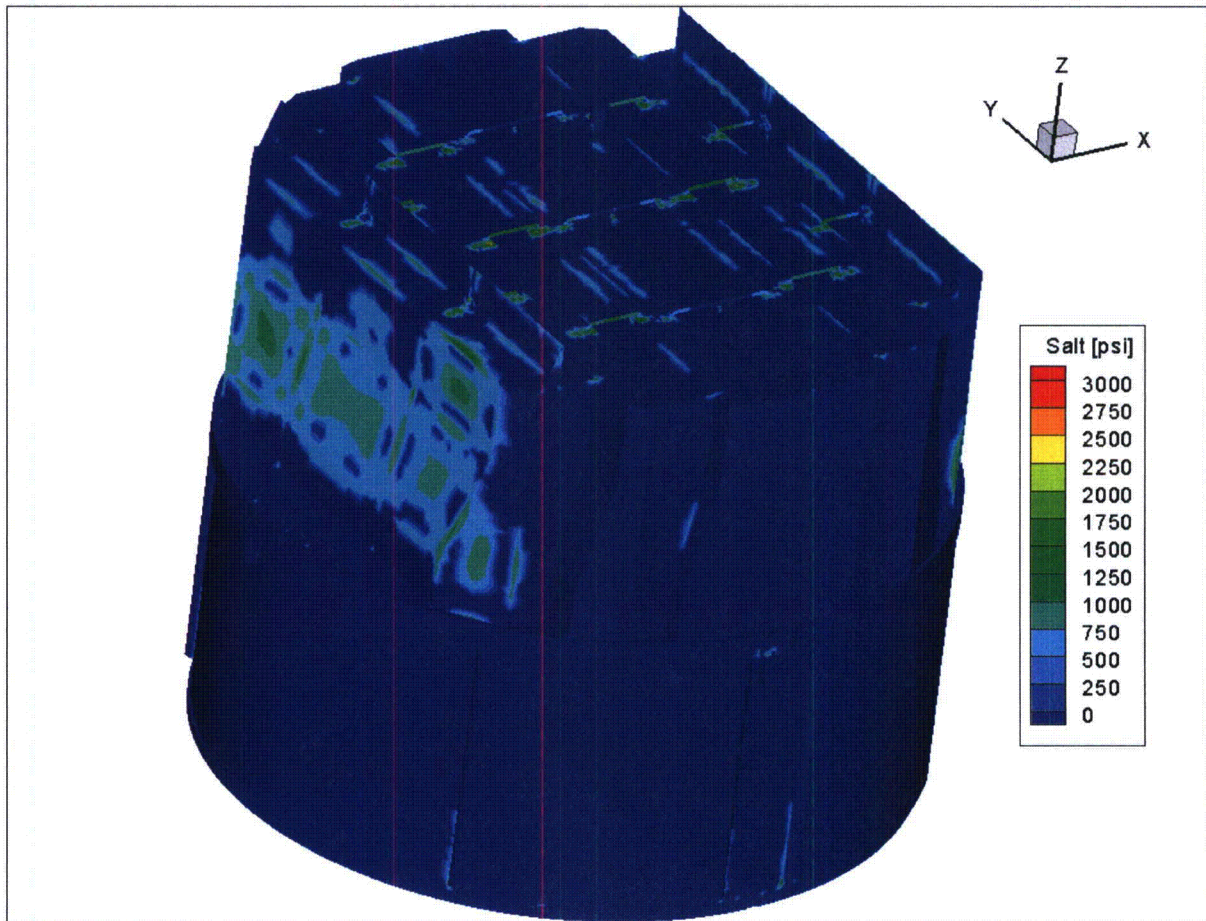


Figure 11d. Contour plot of alternating stress intensity, S_{alt} , for CLTP load. The maximum alternating stress intensity is 3,007 psi.

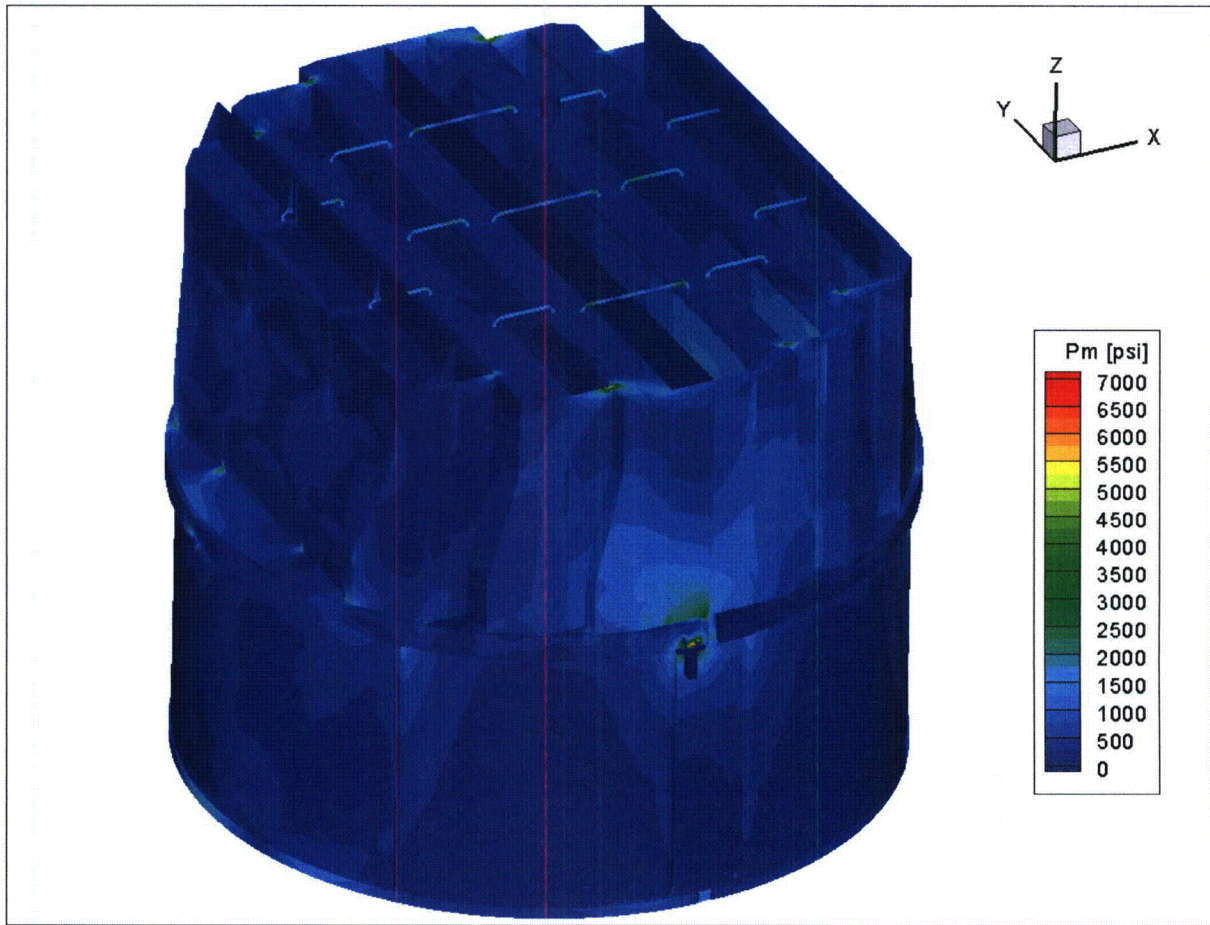


Figure 12a. Contour plot of maximum membrane stress intensity, P_m , for CLTP operation with frequency shifts. The recorded stress at a node is the maximum value taken over all frequency shifts. The maximum stress intensity is 6,865 psi.

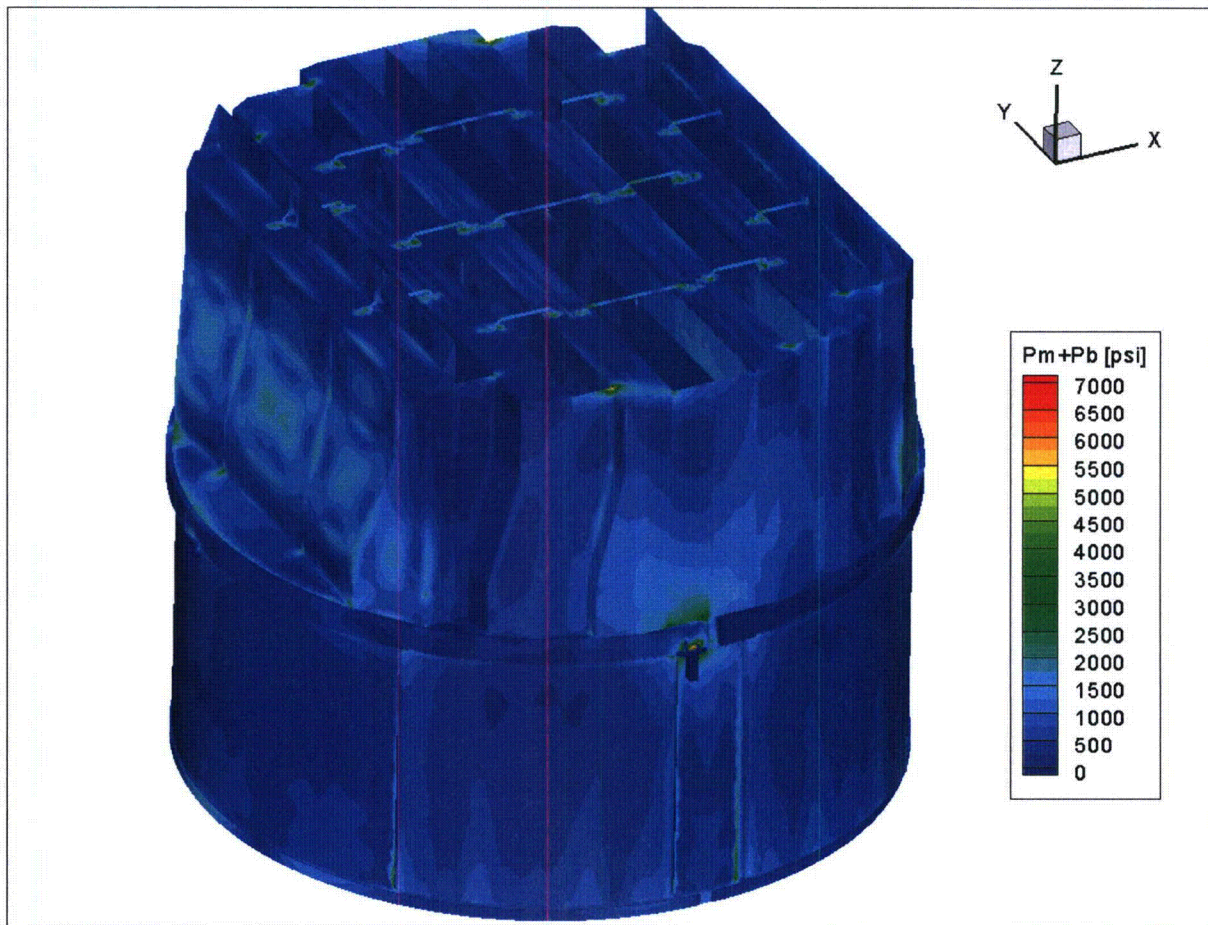


Figure 12b. Contour plot of maximum membrane+bending stress intensity, $P_m + P_b$, for CLTP operation with frequency shifts. The recorded stress at a node is the maximum value taken over all frequency shifts. The maximum stress intensity is 6,865 psi. First view.

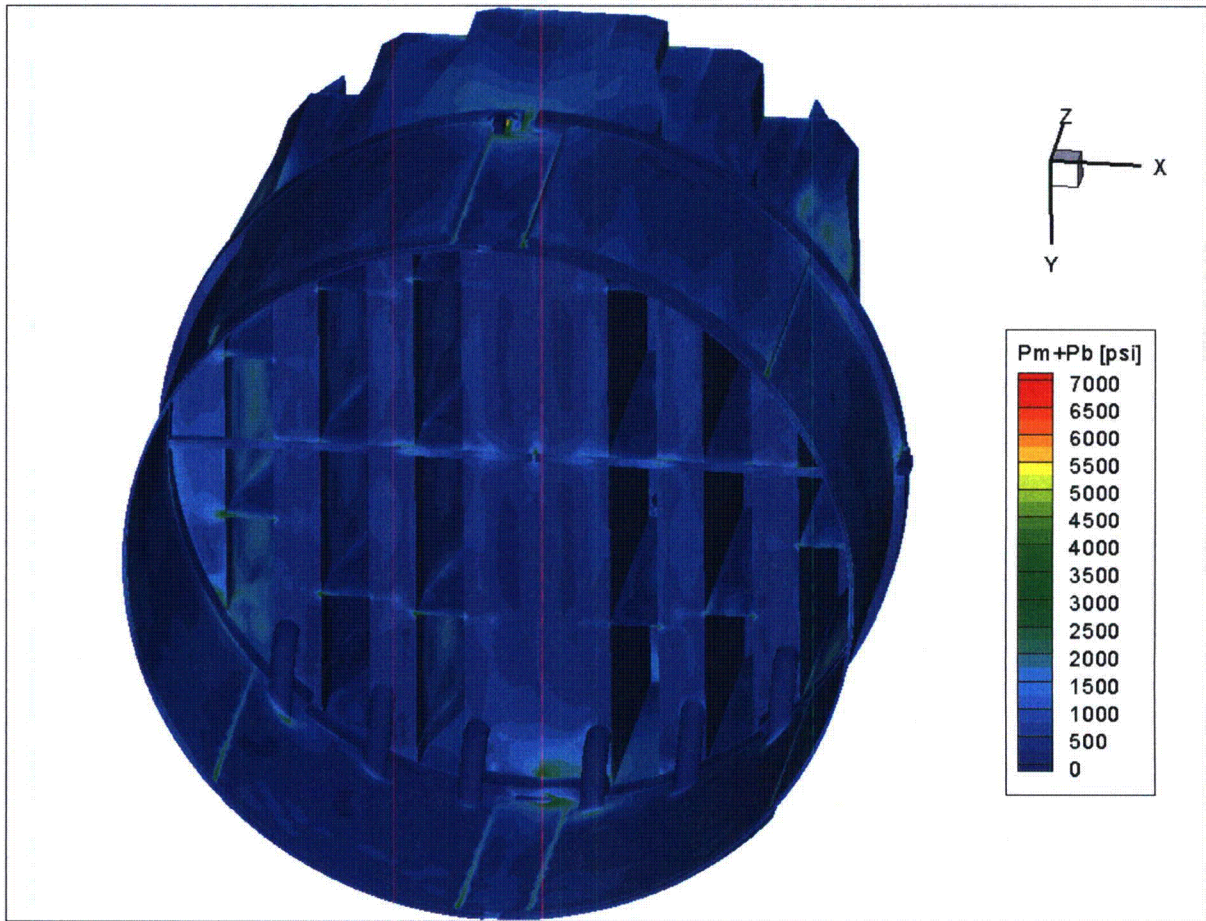


Figure 12c. Contour plot of maximum membrane+bending stress intensity, P_m+P_b , for CLTP operation with frequency shifts. This second view from beneath reveals stresses on the hood supports, support bar, inner base plates and drain pipe/skirt welds.

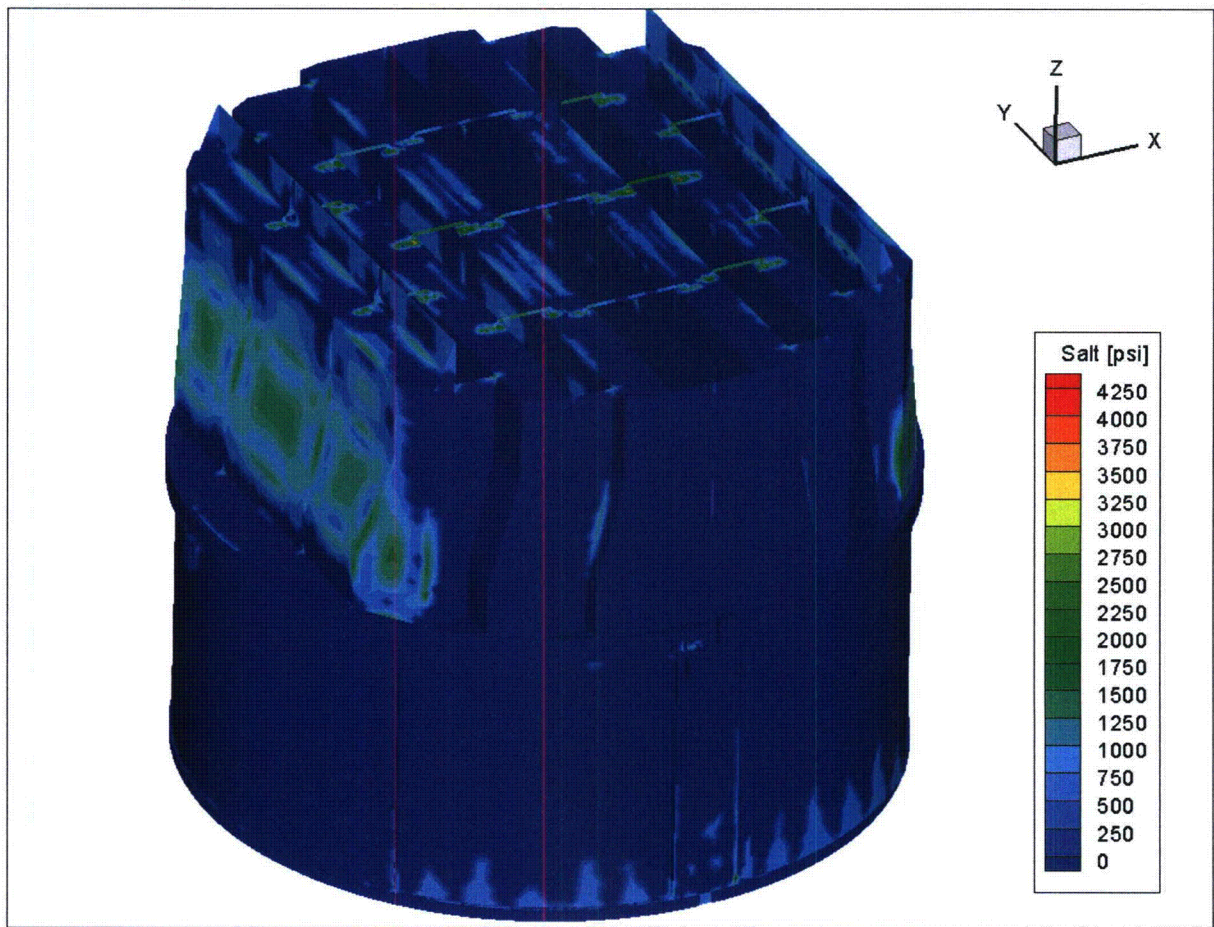


Figure 12d. Contour plot of alternating stress intensity, S_{alt} , for CLTP operation with frequency shifts. The recorded stress at a node is the maximum value taken over all frequency shifts. The maximum alternating stress intensity is 4,163 psi.

5.2 Load Combinations and Allowable Stress Intensities

The stress ratios computed for CLTP at nominal frequency and with frequency shifting are listed in Table 8. The stress ratios are grouped according to type (SR-P for maximum membrane and membrane+bending stress, SR-a for alternating stress) and location (away from welds or on a weld).

For CLTP operation at nominal frequency the minimum stress ratio is identified as a maximum stress, SR-P=1.82, and is recorded on the top of the middle closure plate where it connects to the inner hood. However, this location is only weakly responsive to acoustic loads as can be seen from the high alternating stress ratio at this location (SR-a>6 at all frequency shifts). The minimum alternating stress ratio, SR-a=2.35, occurs on the tie bar base. In fact the first four nodes identified as having the lowest alternating stress ratios all involve tie bar bases (locations 1, 2 and 4 being on the tie bar base weld and location 2, being on the cover plate one element away from the tie bar base). All of these locations lie on welds as summarized in Table 8a and the accompanying Figure 13.

The effects of frequency shifts can be conservatively accounted for by identifying the minimum stress ratio at every node, where the minimum is taken over all the frequency shifts considered (including the nominal or 0% shift case). The resulting stress ratios are then processed as before to identify the smallest stress ratios anywhere on the structure, categorized by stress type (maximum or alternating) and location (on or away from a weld). The results are summarized in Table 8b and show that the lowest stress ratio, SR-a=1.65, is now identified with an alternating stress and occurs at the same location (strictly, at a mirror location) as in the nominal case. This pronounced change in alternating stress ratio (from 2.35 at zero shift) reflects the stronger responsiveness of the tie bar bases to acoustic loads. Moreover, Table 8b shows that the five lowest alternating stress ratios are associated with tie bar bases. The lowest alternating stress ratios away from a tie bar base are SR-a=2.48 (at the middle of the middle tie bar) and SR-a=2.77 at the bottom of the middle hood where it connects to the middle cover plate and hood support (not listed in the table). The smallest stress ratio associated with a maximum stress at any frequency shift is SR-P=1.75 which is only slightly lower than the nominal value.

Finally, the maximum stress intensities at any frequency shift for the locations in Table 8b are recomputed using the CLTP loads without noise removal and reported in Table 8c. Changes in stress ratios are generally small (15% or less). For the lowest alternating stress ratio the change is only 3.6%.

In summary, the lowest alternating stress ratios (all those with SR-a<2) occur on tie bar bases at the +10% frequency shift. The lowest value at any frequency shift is SR-a=1.65 indicating that stresses are well below allowable levels. The lowest stress ratio associated with a maximum stress is SR-P=1.75. This value is dominated by the static component and is only weakly altered by acoustic loads.

Table 8a. Locations with minimum stress ratios for CLTP conditions with no frequency shift. Stress ratios are grouped according to stress type (maximum – SR-P; or alternating – SR-a) and location (away from a weld or at a weld). Bold text indicates minimum stress ratio of any type on the structure. Signal noise has been removed using 19% power data. Locations are depicted in Figure 13.

Stress Ratio	Location	Weld	Location (in.)			node	Stress Intensity (psi)			Stress Ratio	
			x	y	z		Pm	Pm+Pb	S _{alt}	SR-P	SR-a
SR-P	1. USR/Seismic Block/Support Block	No	-122.1	10	-9.5	118466	6813	6813	1460	2.69	8.47
"	2. USR part/Support Block/Support	"	7	122.3	-9.5	118711	6621	6621	1370	2.76	9.03
SR-a	1. lock gusset	No	-77	31.4	91.9	93557	2120	4872	3007	5.63	4.11
SR-P	1. Top Cover Inner Hood/Middle Closure Plate/Inner Hood	Yes	31.5	108.4	88.9	96687	5539	6117	876	1.82	7.84
"	2. Splice Bar/USR part	"	2.2	119	0	118662	5198	5198	<500	1.94	>13
"	3. Middle Cover Plate/Hood Support/Inner Hood	"	-39.8	59.8	0	98204	4650	4655	1269	2.16	5.41
"	4. USR Part/Support Block/Support	"	-8.5	-122.2	-9.5	118337	3999	3999	502	2.52	13.67
"	5. Middle Cover Plate/Hood Support/Middle Hood	"	-70.8	54.6	0	99362	3974	3995	1424	2.53	4.82
SR-a	1. Top Cover/Top Tie Bar Base	Yes	-48	3	88.9	92532	390	3385	2925	4.46	2.35
"	2. Top Cover Inner Hood/Top Perf. Plate/Top Cover Overlap	"	-24	2.8	88.9	90207	604	2394	2366	6.31	2.9
"	3. Top Cover/Top Tie Bar Base	"	-83.8	-31.8	88.9	103481	205	2719	2364	5.55	2.91
"	4. Top Cover/Top Tie Bar Base	"	-48	-58.6	88.9	97521	226	2634	2240	5.73	3.07
"	5. Outer Side Panel/Vane Bank Thin/Vane Bank Thick/Outer End Wall	"	86	85	12.1	101181	487	2343	2015	6.44	3.41

See Table 7a for coordinates description.

Table 8b. Locations with minimum stress ratios for CLTP conditions with frequency shifts. Stress ratios at every node are recorded as the lowest stress ratio identified during the frequency shifts. Stress ratios are grouped according to stress type (maximum – SR-P; or alternating – SR-a) and location (away from a weld or at a weld). Signal noise has been removed using 19% power data. Bold text indicates minimum stress ratio of any type on the structure. Locations are depicted in Figure 14.

Stress Ratio	Location	Weld	Location (in.)			node	Stress Intensity (psi)			Stress Ratio		% Freq. Shift
			x	y	z		Pm	Pm+Pb	S _{alt}	SR-P	SR-a	
SR-P	1. USR part/Support Block/Support	No	7	122.3	-9.5	118711	6865	6865	1571	2.67	7.87	-10
"	2. USR/Seismic Block/Support Block	"	-122.1	10	-9.5	118466	6813	6813	1460	2.69	8.47	0
SR-a	1. Lock/Lock Gusset	No	-77	31.4	91.9	93557	2505	6121	4104	4.48	3.01	+10
"	2. Top Cover	"	-52.9	3.9	88.9	23911	401	3261	2808	8.42	4.4	+10
SR-P	1. Top Cover Inner Hood/Middle Closure Plate/Inner Hood	"	31.5	108.4	88.9	96687	5735	6337	1090	1.75	6.3	+2.5
"	2. Splice Bar/USR part	"	2.2	119	0	118662	5359	5359	656	1.88	10.47	+10
"	3. Middle Cover Plate/Hood Support/Inner Hood	"	-39.8	59.8	0	98204	4991	5037	1673	2.02	4.1	+10
"	4. USR Part/Support Block/Support	"	-8.5	-122.2	-9.5	118337	4187	4187	639	2.4	10.75	10
"	5. Middle Cover Plate/Hood Support/Middle Hood	"	70.8	-54.6	0	95987	4106	4293	1755	2.45	3.91	2.5
SR-a	1. Top Cover/Top Tie Bar Base	Yes	48	3	88.9	96745	396	4582	4163	3.29	1.65	+10
"	2. Top Cover Inner Hood/Top Cover Overlap/Top Perf. Plate	"	24	2.8	88.9	88313	704	3812	3693	3.96	1.86	+10
"	3. Top Cover/Top Tie Bar Base	"	48	-58.6	88.9	97260	355	4147	3462	3.64	1.98	+10
"	4. Top Cover/Top Tie Bar Base	"	-81.5	30.2	88.9	107776	679	3634	2890	4.15	2.38	+5
"	5. Top Cover Inner Hood/Hood Support/Top Tie Bar Base	"	28.2	-59.9	88.9	100330	689	3402	2816	4.44	2.44	+10
"	6. Mid Plate/Top Tie Bar Mid	"	0	2.2	88.9	88299	395	2932	2767	5.15	2.48	+7.5
"	7. Top Cover Middle Hood/Top Perf/Top Cover Overlap	"	-55	31.6	88.9	107924	365	3568	2680	4.23	2.56	+10

See Table 7a for coordinates description.

Table 8c. Minimum stress stress ratios at any frequency shift for the nodes listed in Table 8b computed using the unfiltered CLTP loads (i.e., signal noise has *not* been removed). Locations are depicted in Figure 14.

Stress Ratio	Location	Weld	Location (in.)			node	Stress Intensity (psi)			Stress Ratio		% Freq. Shift
			x	y	z		Pm	Pm+Pb	S _{alt}	SR-P	SR-a	
SR-P	1. USR part/Support Block/Support	No	7	122.3	-9.5	118711	6859	6859	1583	2.67	7.81	-10
"	2. USR/Seismic Block/Support Block	"	-122.1	10	-9.5	118466	6952	6952	1560	2.63	7.92	0
SR-a	1. Lock/Lock Gusset	No	-77	31.4	91.9	93557	2991	6200	4399	4.43	2.81	+10
"	2. Top Cover	"	-52.9	3.9	88.9	23911	436	3377	2969	8.13	4.16	+10
SR-P	1. Top Cover Inner Hood/Middle Closure Plate/Inner Hood	"	31.5	108.4	88.9	96687	5930	6538	1246	1.70	5.51	+10
"	2. Splice Bar/USR part	"	2.2	119	0	118662	5377	5377	664	1.87	10.34	+10
"	3. Middle Cover Plate/Hood Support/Inner Hood	"	-39.8	59.8	0	98204	5110	5205	1985	1.97	3.46	+7.5
"	4. USR Part/Support Block/Support	"	-8.5	-122.2	-9.5	118337	4211	4211	652	2.39	10.54	+10
"	5. Middle Cover Plate/Hood Support/Middle Hood	"	70.8	-54.6	0	95987	4616	5819	3107	2.18	2.21	+2.5
SR-a	1. Top Cover/Top Tie Bar Base	Yes	48	3	88.9	96745	514	4678	4315	3.23	1.59	+10
"	2. Top Cover Inner Hood/Top Cover Overlap/Top Perf. Plate	"	24	2.8	88.9	88313	727	3878	3786	3.89	1.81	+10
"	3. Top Cover/Top Tie Bar Base	"	48	-58.6	88.9	97260	497	4252	3578	3.55	1.92	+10
"	4. Top Cover/Top Tie Bar Base	"	-81.5	30.2	88.9	107776	778	3857	3250	3.91	2.11	+5
"	5. Top Cover Inner Hood/Hood Support/Top Tie Bar Base	"	28.2	-59.9	88.9	100330	919	3467	2881	4.36	2.38	+10
"	6. Mid Plate/Top Tie Bar Mid	"	0	2.2	88.9	88299	405	3208	2912	4.71	2.36	+7.5
"	7. Top Cover Middle Hood/Top Perf/Top Cover Overlap	"	-55	31.6	88.9	107924	388	3742	2807	4.03	2.45	+10

See Table 7a for coordinates description.

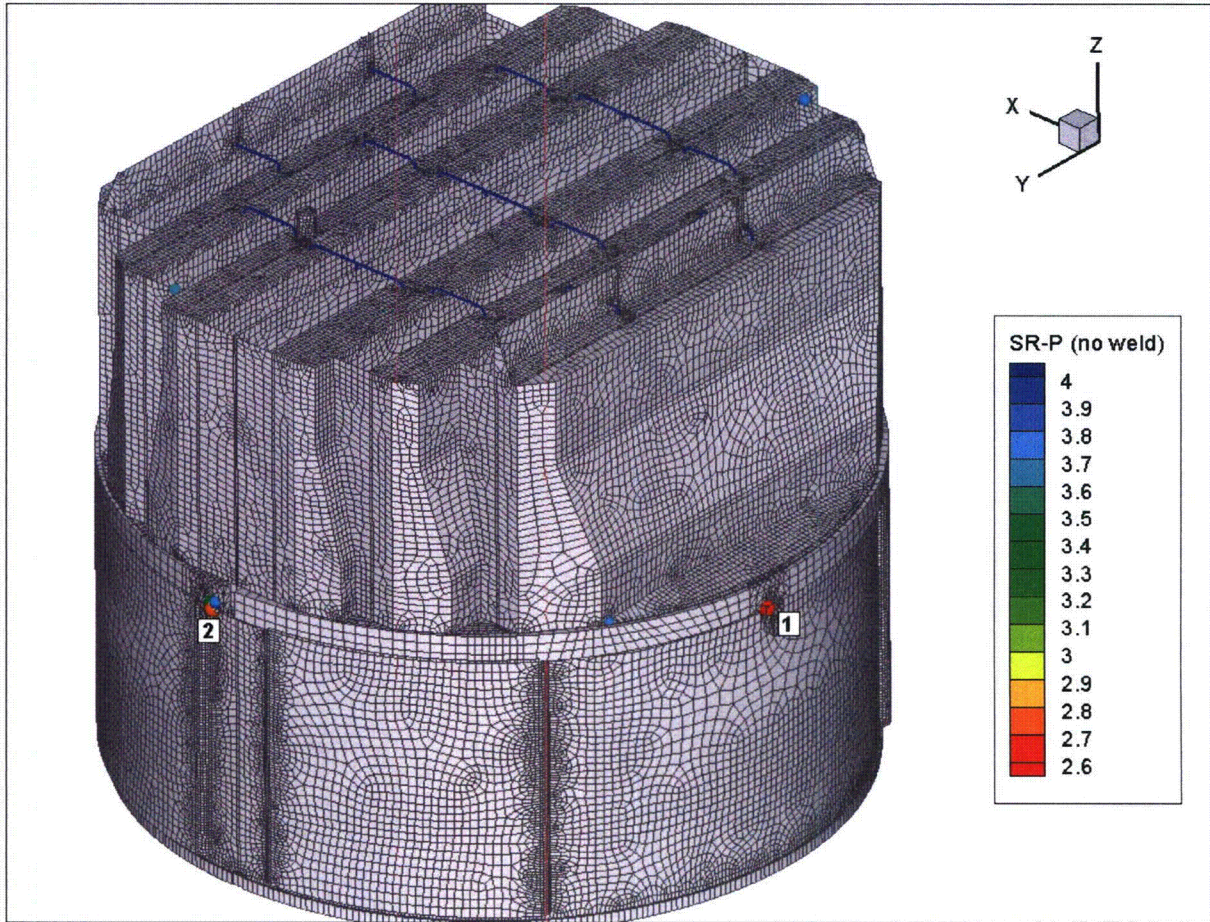


Figure 13a. Locations of nodes with stress ratios, $SR-P \leq 4$, associated with a maximum stress at non-welds for nominal CLTP operation. Numbers refers to the enumerated locations for SR-P values at non-welds in Table 8a.

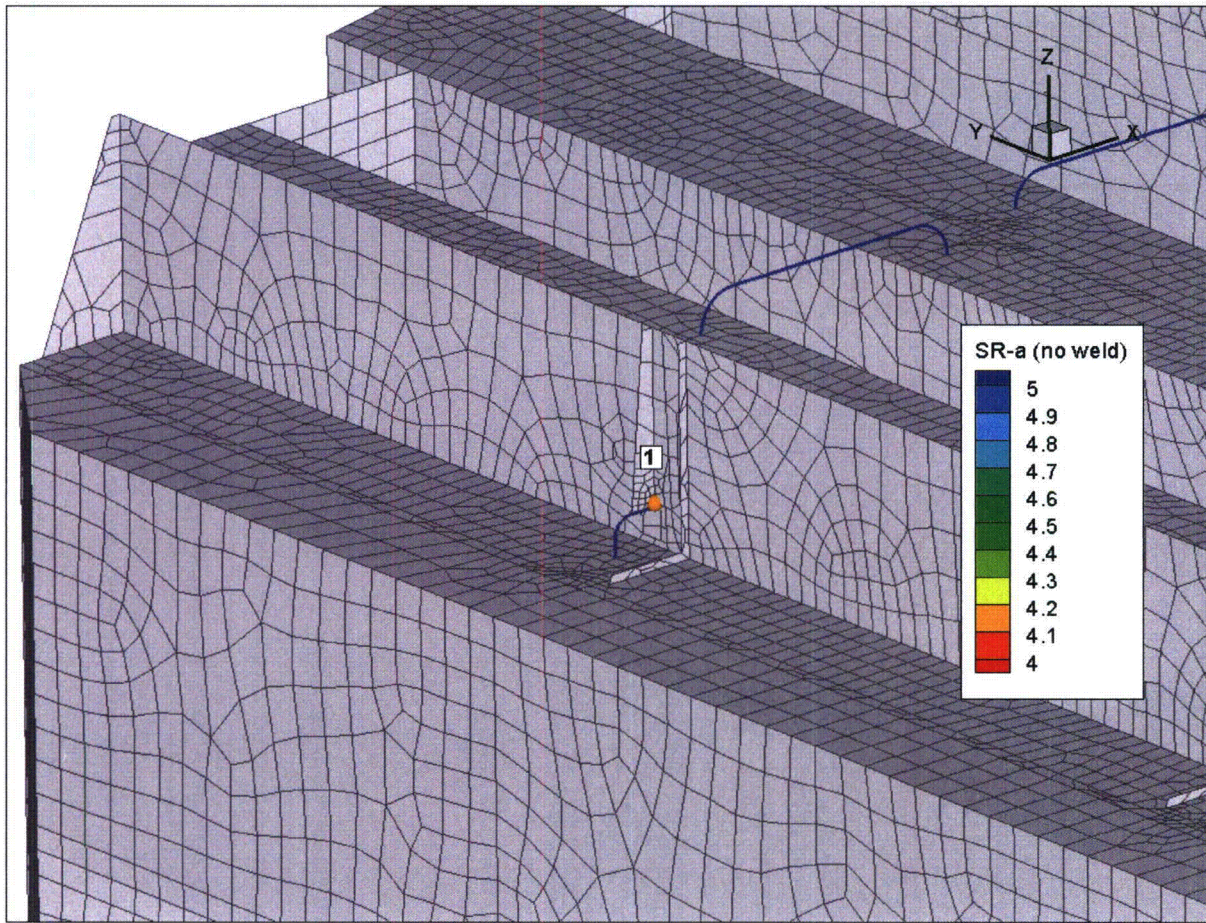


Figure 13b. Location of minimum alternating stress ratios, $SR-a \leq 5$, at non-welds for nominal CLTP operation. Number refers to the enumerated locations for SR-a values at non-welds in Table 8a.

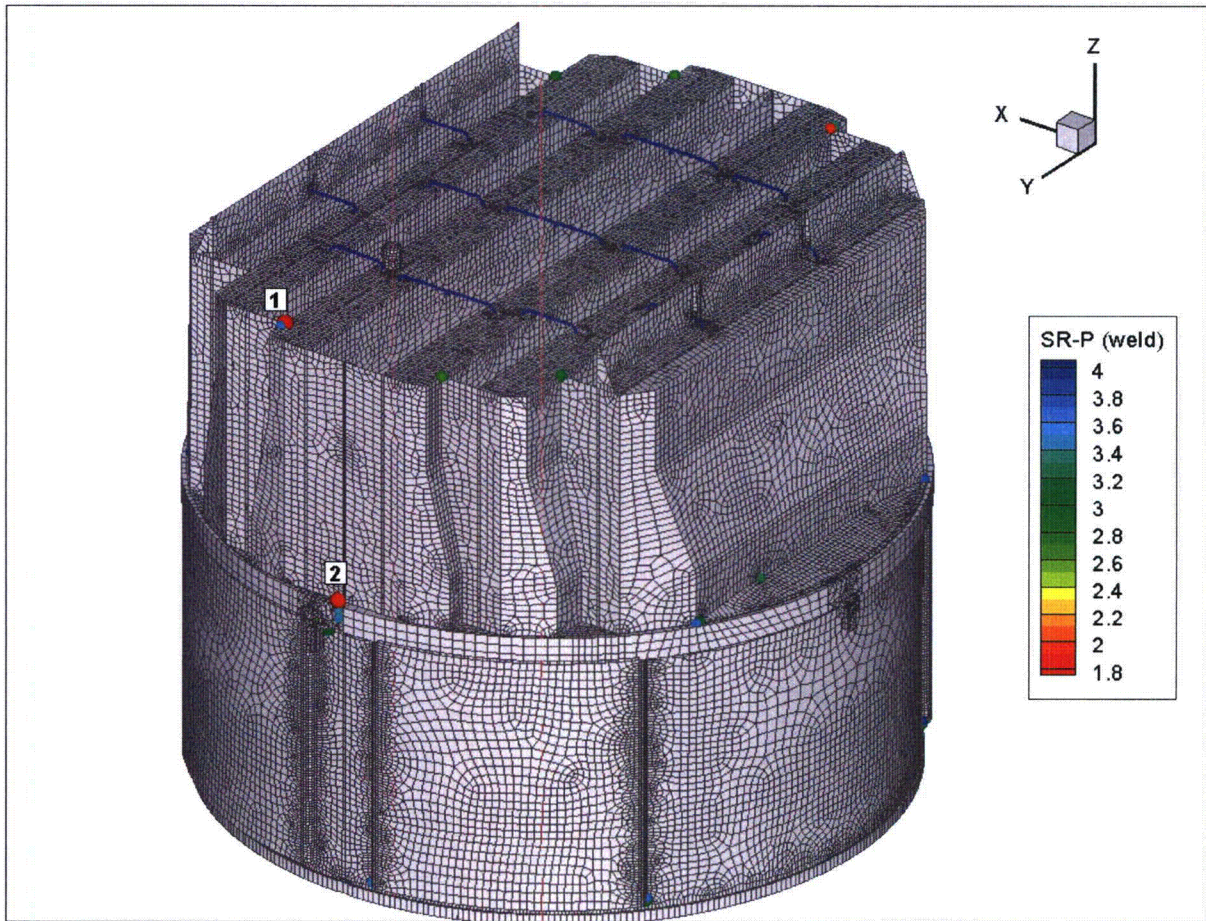


Figure 13c. Locations of smallest stress ratios, $SR-P \leq 4$, associated with maximum stresses at welds for nominal CLTP operation. Numbers refer to the enumerated locations for SR-P values at welds in Table 8a. This view shows locations 1 and 2.

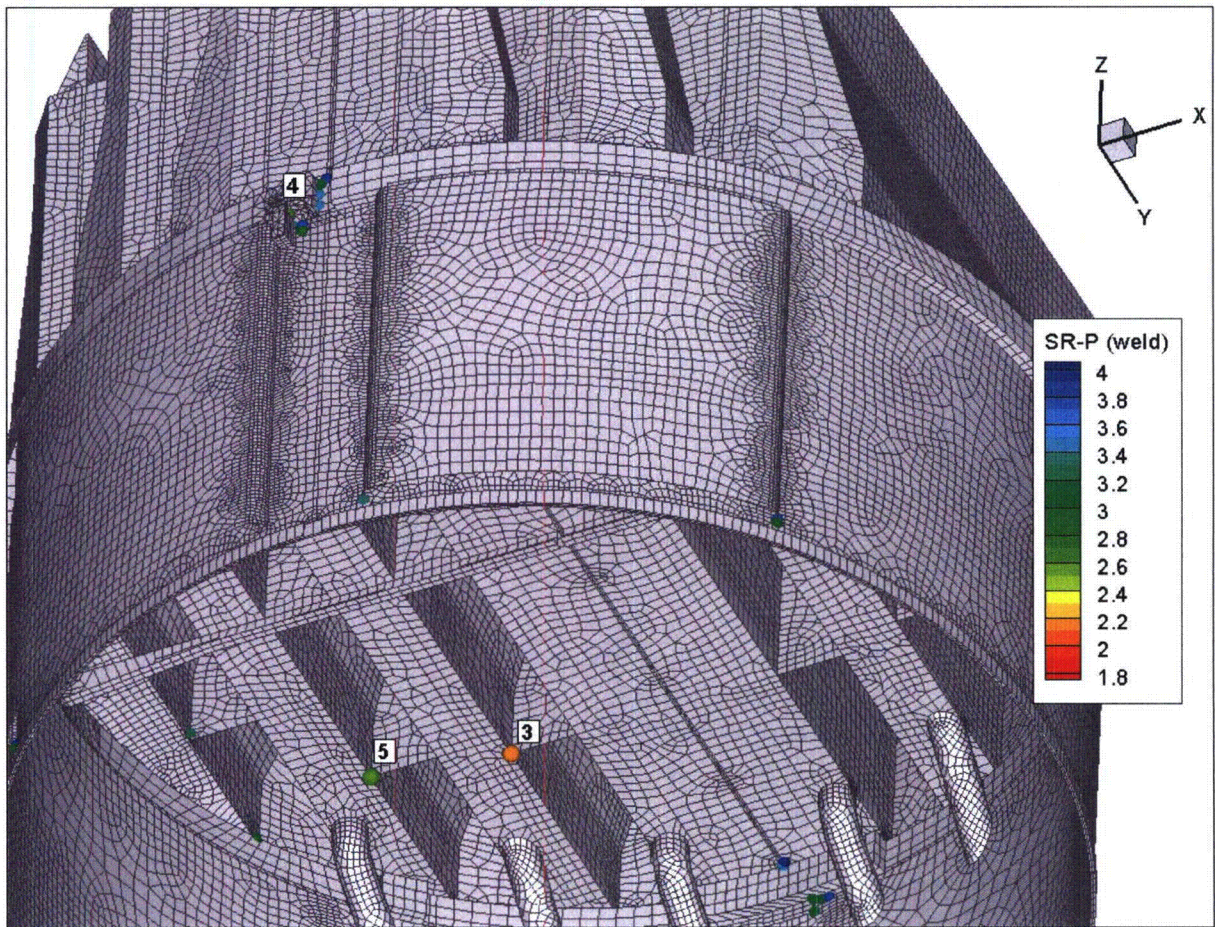


Figure 13d. Locations of minimum stress ratios, $SR-P \leq 4$, associated with maximum stresses at welds for nominal CLTP operation. Numbers refer to the enumerated locations for SR-P values at welds in Table 8a. This view shows locations 3-5.

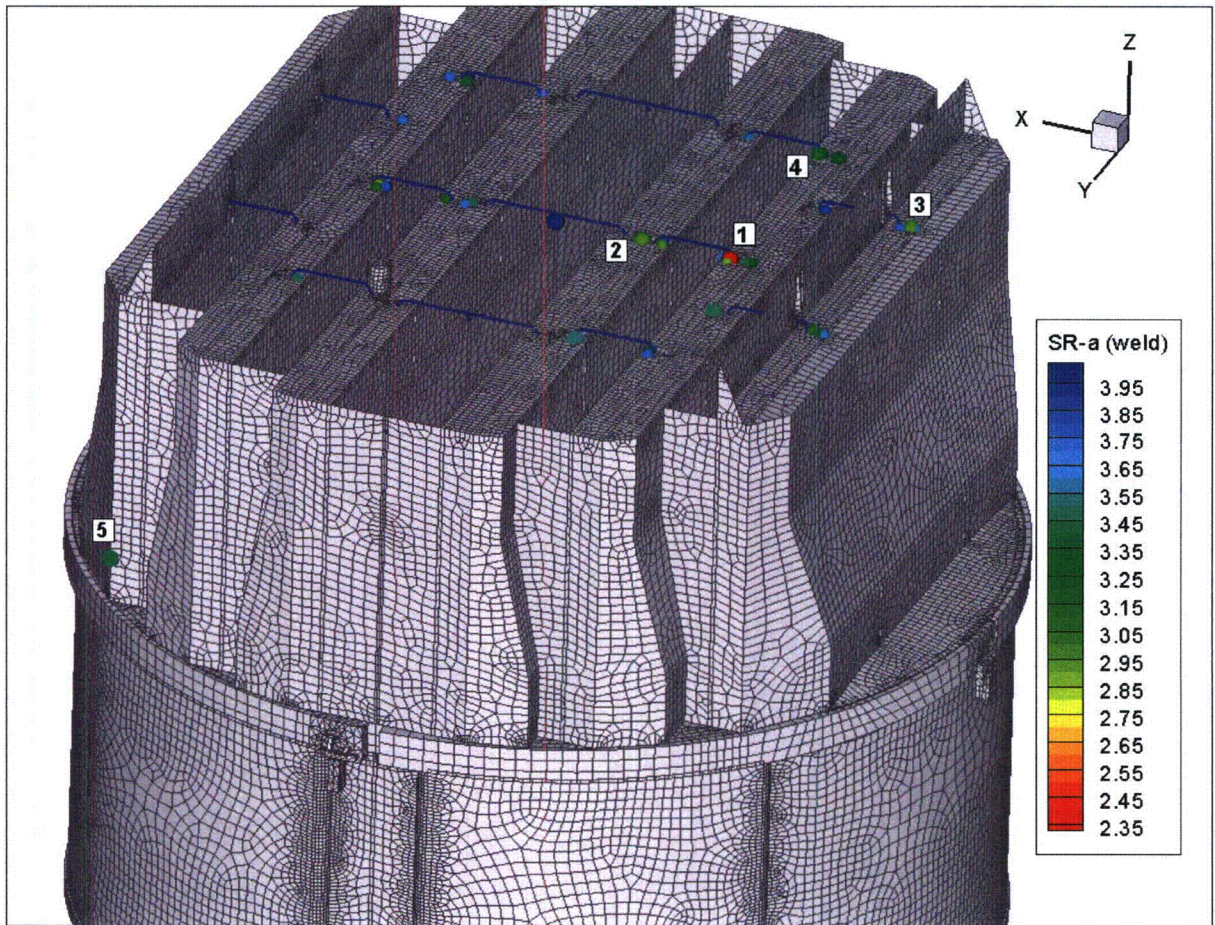


Figure 13e. Locations of minimum alternating stress ratios, $SR-a \leq 4$, at welds for nominal CLTP operation. Numbers refer to the enumerated locations for SR-a values at welds in Table 8a. Locations 1-5 are shown.

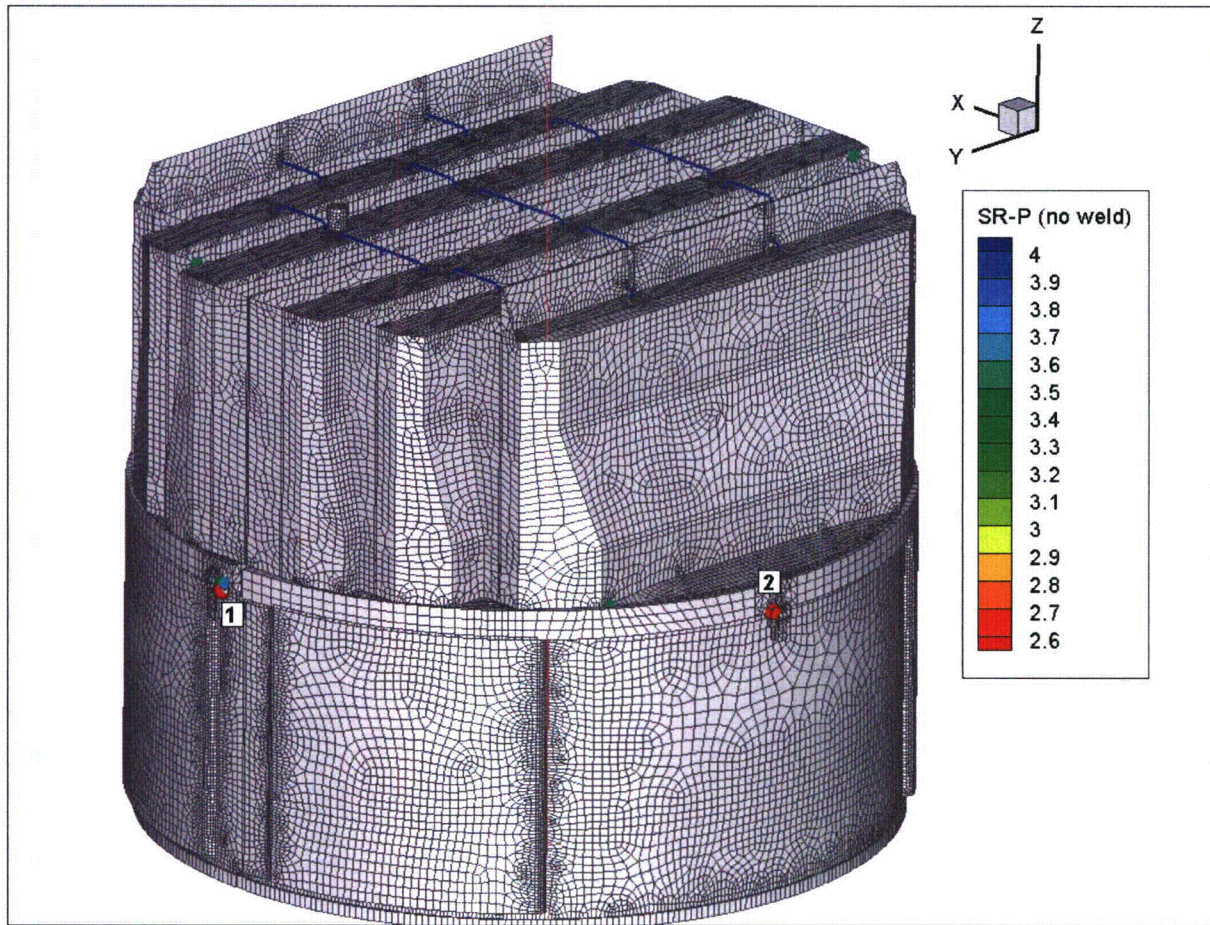


Figure 14a. Locations of minimum stress ratios, $SR-P \leq 4$, associated with maximum stresses at non-welds for CLTP operation with frequency shifts. The recorded stress ratio is the minimum value taken over all frequency shifts. The numbers refers to the enumerated location for SR-P values at non-welds in Table 8b.

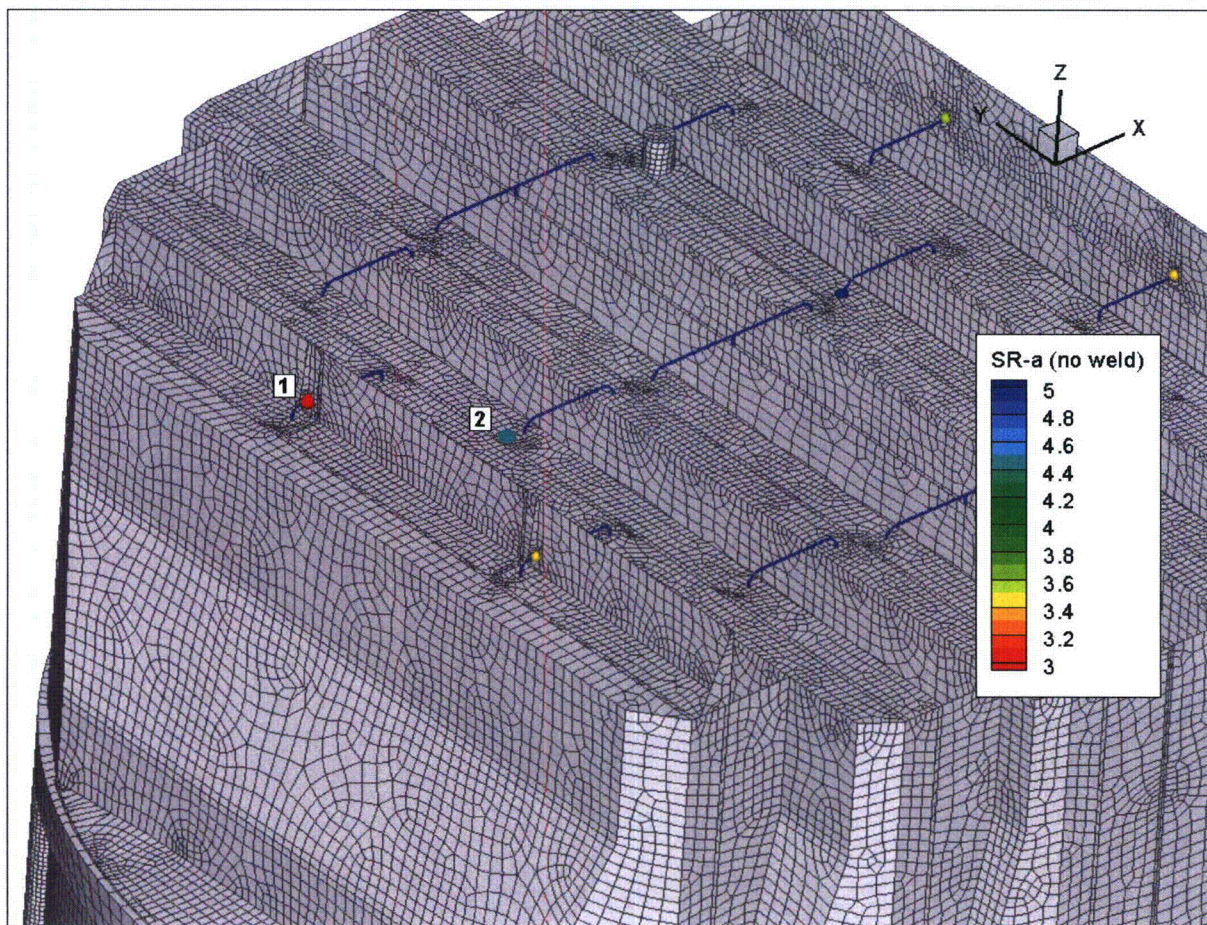


Figure 14b. Locations of minimum alternating stress ratios, $SR-a \leq 5$, at non-welds for CLTP operation with frequency shifts. The recorded stress ratio at a node is the minimum value taken over all frequency shifts. Numbers refer to the enumerated locations for $SR-a$ values at non-welds in Table 8b.

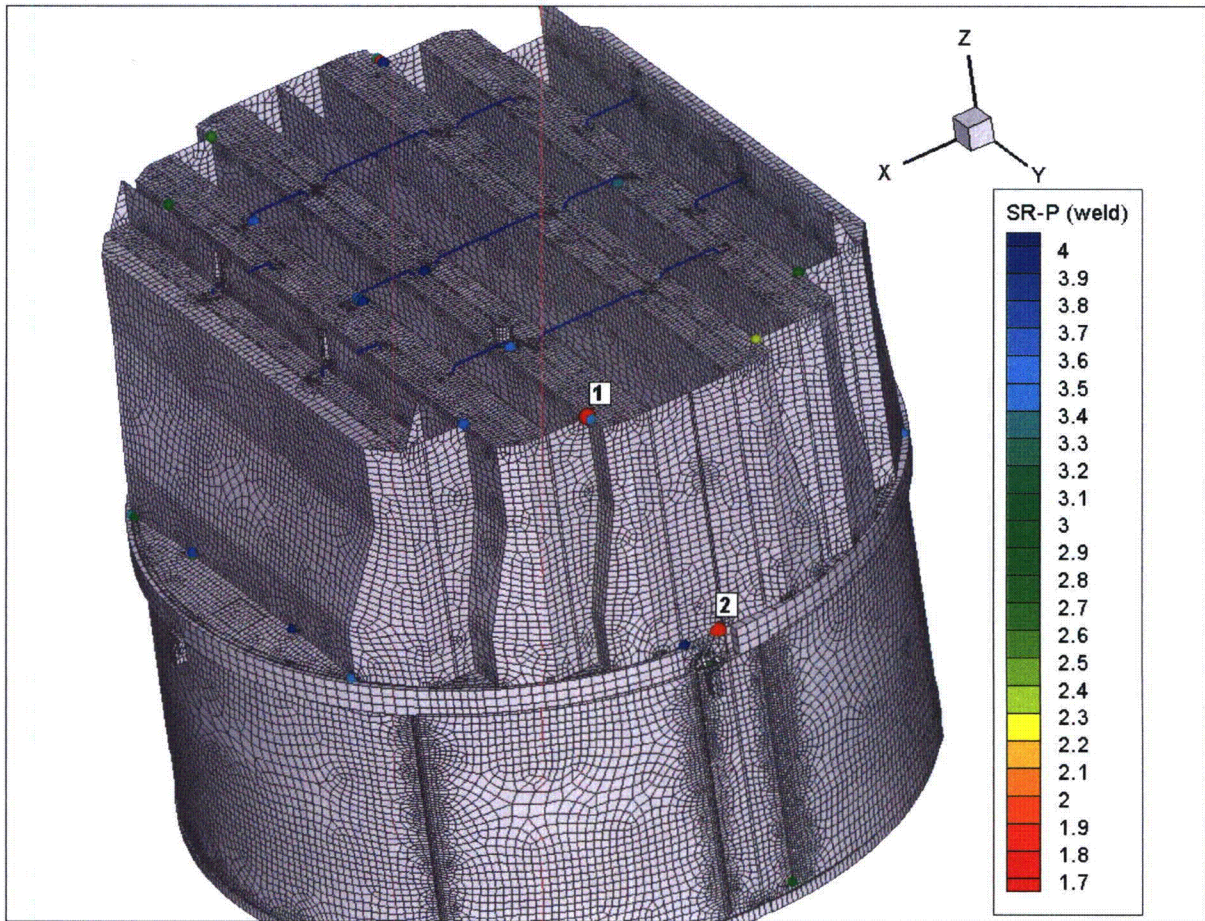


Figure 14c. Locations of minimum stress ratios, $SR-P \leq 4$, associated with maximum stresses at welds for CLTP operation with frequency shifts. The recorded stress ratio at a node is the minimum value taken over all frequency shifts. Numbers refer to the enumerated locations for SR-P values at welds in Table 8b. This view shows locations 1 and 2.

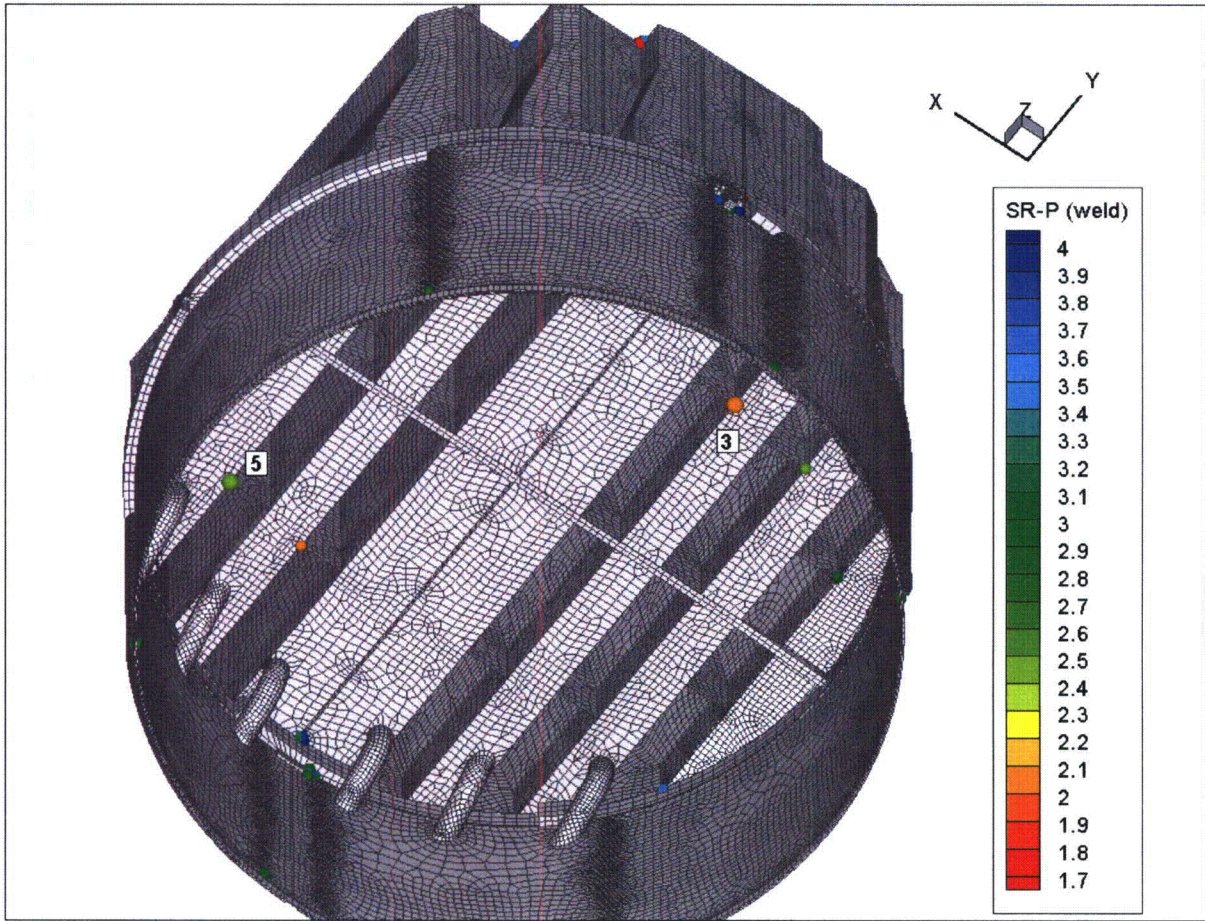


Figure 14d. Locations of minimum stress ratios, $SR-P \leq 4$, associated with maximum stresses at welds for CLTP operation with frequency shifts. The recorded stress ratio at a node is the minimum value taken over all frequency shifts. Numbers refer to the enumerated locations for SR-P values at welds in Table 8b. This view shows locations 3 and 5.

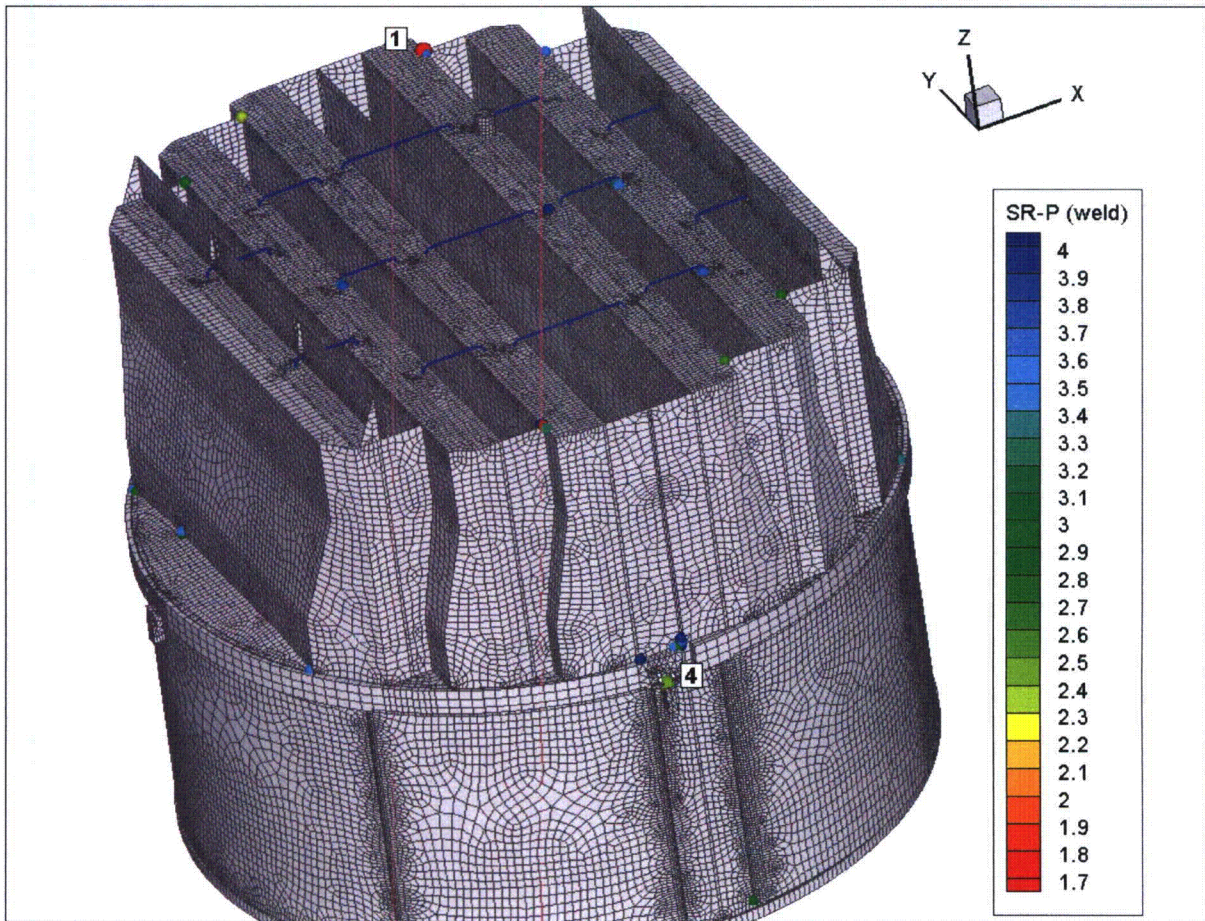


Figure 14e. Locations of minimum stress ratios, $SR-P \leq 4$, associated with maximum stresses at welds for CLTP operation with frequency shifts. The recorded stress ratio at a node is the minimum value taken over all frequency shifts. Numbers refer to the enumerated locations for SR-P values at welds in Table 8b. This view shows locations 1 and 4.

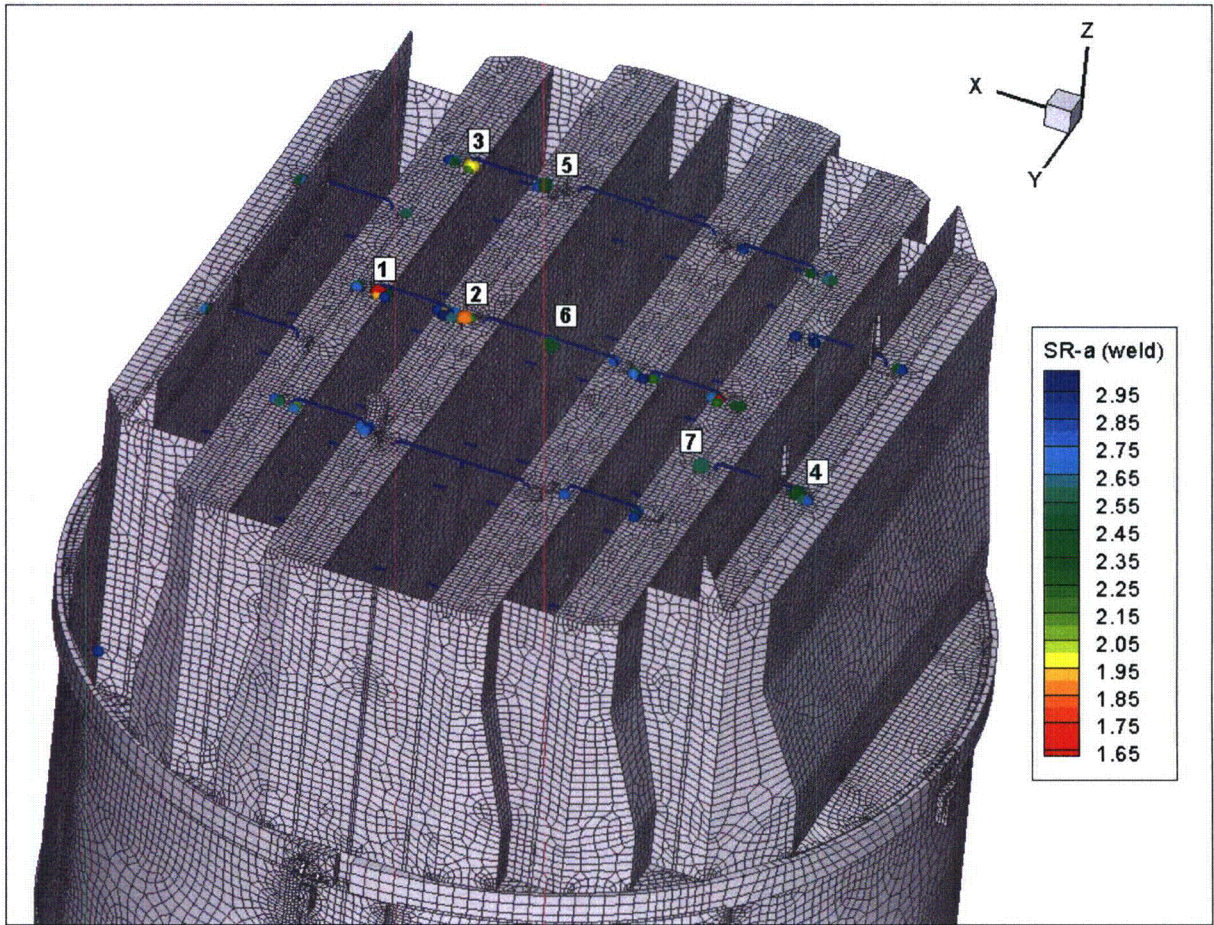


Figure 14f. Locations of minimum alternating stress ratios, $SR-a \leq 3$, at welds for CLTP operation with frequency shifts. The recorded stress ratio at a node is the minimum value taken over all frequency shifts. Numbers refer to the enumerated locations for SR-a values at welds in Table 8b.

5.3 Frequency Content and Filtering of the Stress Signals

The frequency contribution to the stresses can be investigated by examining the power spectral density (PSD) curves and accumulative PSDs for selected nodes having low alternating stress ratios. The accumulative PSDs are computed directly from the Fourier coefficients as

$$\Sigma(\omega_n) = \sqrt{\sum_{k=1}^n |\tilde{\sigma}(\omega_k)|^2}$$

where $\tilde{\sigma}(\omega_k)$ is the complex stress harmonic at frequency, ω_k . Accumulative PSD plots are useful for determining the frequency components and frequency ranges that make the largest contributions to the fluctuating stress. Unlike PSD plots, no “binning” or smoothing of frequency components is needed to obtain smooth curves. Steep step-like rises in $\Sigma(\omega)$ indicate the presence of a strong component at a discrete frequency whereas gradual increases in the curve imply significant content over a broader frequency range. From Parseval’s theorem, equality between $\Sigma(\omega_N)$ (where N is the total number of frequency components) and the RMS of the stress signal in the time domain is established.

The selected nodes are the ones having the lowest alternating stress ratios (at a weld) in Table 8b. These are:

- Node 96,745 – located on the weld connecting the base of the central tie bar to the top vane bank cover plate of the middle hood. The associated PSDs are shown in Figure 15a.
- Node 88,313 - located on the weld where the entry perforated plate meets the top vane bank cover plate of the inner hood. The associated PSDs are shown in Figure 15b.
- Node 97,260 – located on the weld connecting the base of an outer tie bar to the top vane bank cover plate of the middle hood. The associated PSDs are shown in Figure 15c.
- Node 107776 – located on the weld connecting the base of a tie bar to the top vane bank cover plate of the outer hood. The associated PSDs are shown in Figure 15d.

In each case, since there are six stress components and up to three different section locations for shells (the top, mid and bottom surfaces), there is a total of 18 stress histories per component. Moreover, at junctions there are at least two components that meet at the junction. The particular stress component that is plotted is chosen as follows. First, the component and section location (top/mid/bottom) is taken as the one that has the highest alternating stress. This narrows the selection to six components. Of these, the component having the highest Root Mean Square (RMS) is selected.

These curves show that the biggest increases in the accumulative PSDs tend to occur at lower frequencies (less than 75 Hz). For all nodes, peaks in the PSD curves occur at 37 Hz, 49 Hz and 58 Hz. Shifting the frequency of the applied load shifts does not shift the peaks appreciably, but alters their magnitudes. This is indicative of particular steam dryer modes being excited by broad band acoustic forcing (in the converse case where a 'spike' in the applied forcing is applied to the structure the peak would be more likely to move). Shifting the frequency results in a stronger forcing of these modes.

Since acoustic loads scale roughly with the square of the steam flow, it is reasonable to anticipate that under EPU conditions (where steam flow increases by 15%) the stresses would increase by approximately $(1.15)^2=1.32$. Under this assumption the minimum alternating stress ratio would reduce from 1.65 to $1.65/1.32=1.25$, which given that the applied loads already account for all end-to-end biases and uncertainties, still contains sufficient margin for sustained EPU operation.

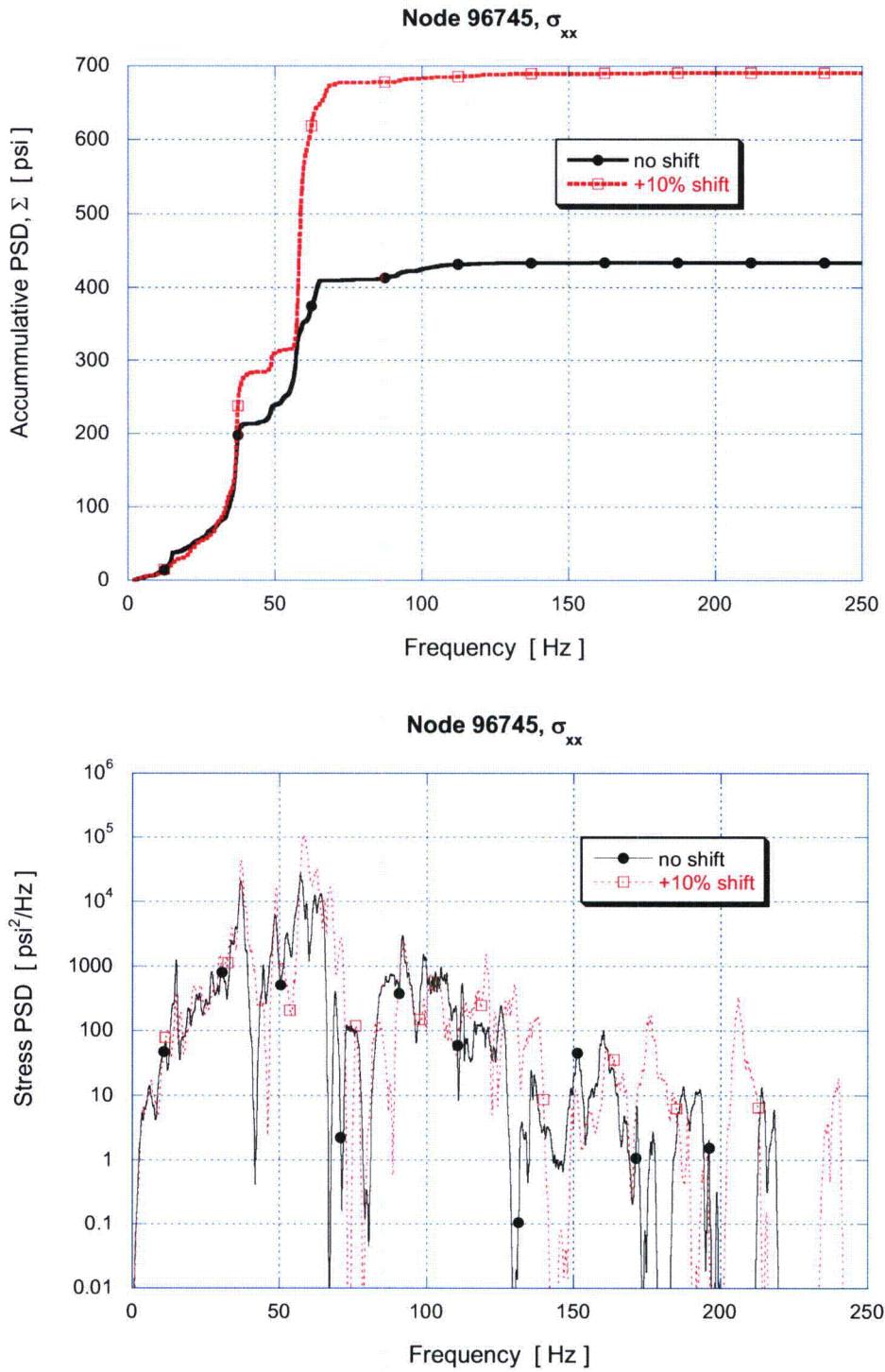


Figure 15a. Accumulative PSD and PSD curves of the σ_{xx} stress response at node 96,745.

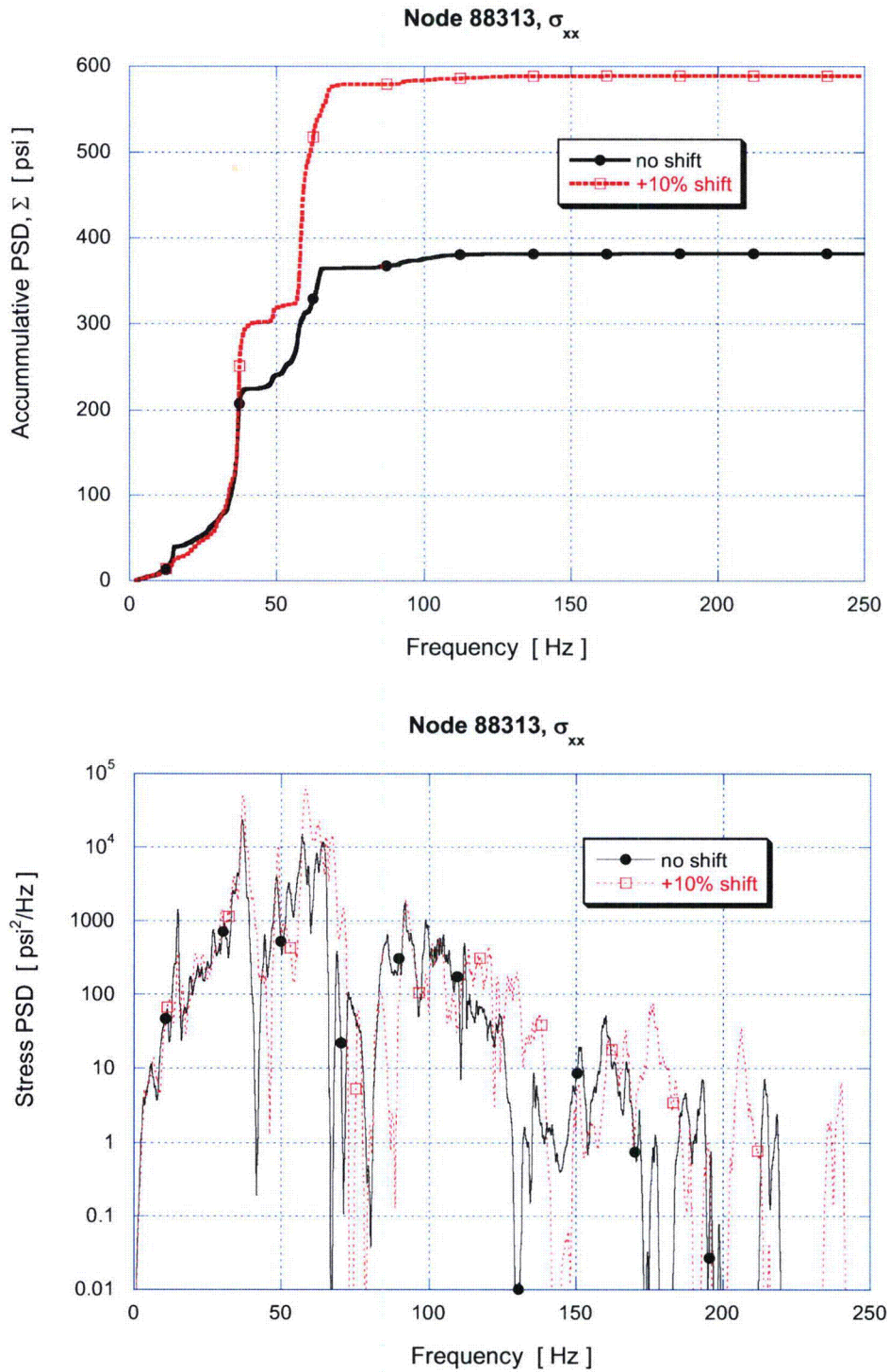


Figure 15b. Accumulative PSD and PSD of the σ_{xx} stress response at node 88,313.

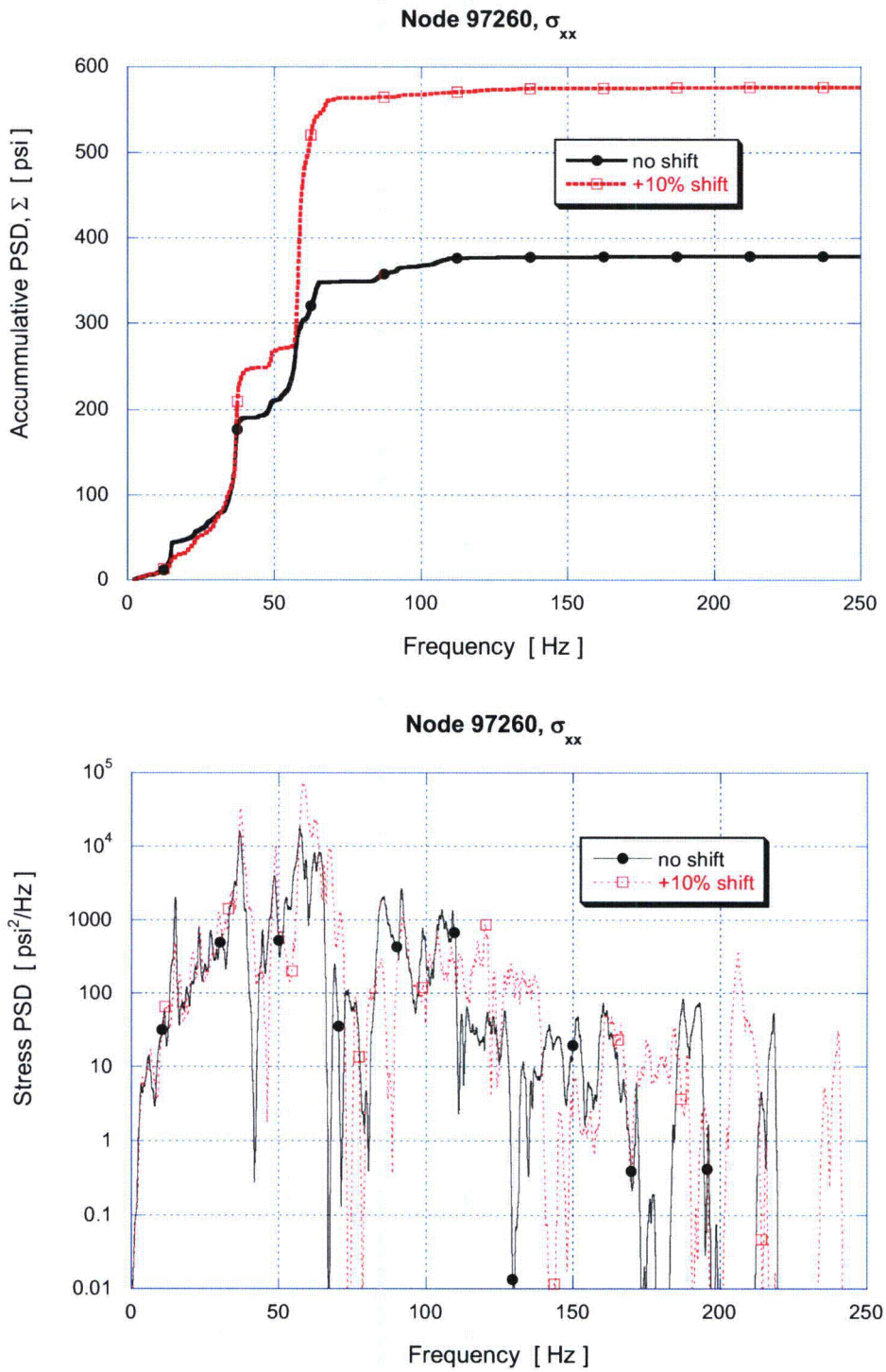


Figure 15c. Accumulative PSD and PSD of the σ_{xx} stress response at node 97,260.

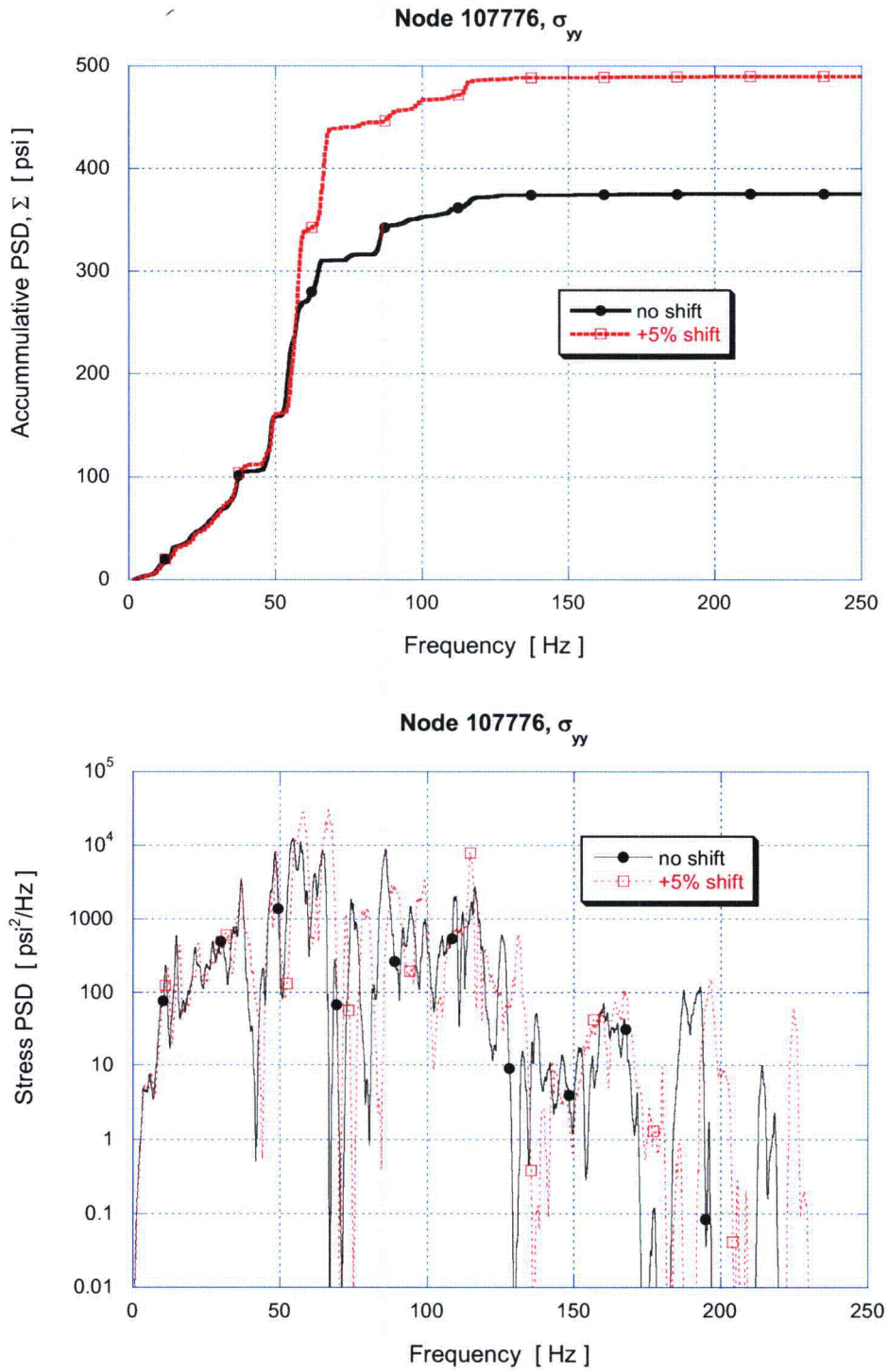


Figure 15d. Accumulative PSD and PSD of the σ_{xx} stress response at node 107,776.

6. Conclusions

A frequency-based steam dryer stress analysis has been used to calculate high stress locations and calculated / allowable stress ratios for the Browns Ferry Unit 2 steam dryer at CLTP load conditions using plant measurement data. A detailed description of the frequency-based methodology and the finite element model for the BFN Unit 2 steam dryer is presented. The CLTP loads obtained in a separate acoustic circuit model [2] including end-to-end bias and uncertainty for both the ACM [2] and FEA were applied to a finite element model of the steam dryer consisting mainly of the ANSYS Shell 63 elements, brick continuum elements and beam elements.

The CLTP loads are applied with compensation for background noise based on 1000 psig data taken at 19% power. The resulting stress histories were analyzed to obtain maximum and alternating stresses at all nodes for comparison against allowable levels. These results are tabulated in Table 8 of this report. The minimum alternating stress ratio at nominal operation is $SR-a=2.35$ and the minimum stress ratio taken over all frequency shifts is $SR-a=1.65$. The maximum stress ratio associated with maximum stress intensities varies weakly with frequency shift and assumes a minimum value of $SR-P=1.82$ at zero shift and $SR-P=1.75$ when all frequency shifts are considered.

On the basis of these CLTP plant loads, the dynamic analysis of the steam dryer shows that the combined acoustic, hydrodynamic and gravity loads produce the following minimum stress ratios:

Frequency Shift	Minimum Stress Ratio	
	Max. Stress, SR-P	Alternating Stress, SR-a
0% (nominal)	1.82	2.35
-10%	1.82	2.38
-7.5%	1.80	2.91
-5%	1.84	2.90
-2.5%	1.82	2.91
+2.5%	1.75	1.90
+5%	1.78	1.87
+7.5%	1.78	1.77
+10%	1.77	1.65
All shifts	1.75 – 1.84	1.65 – 2.91

7. References

1. Continuum Dynamics, Inc. (2005). "Methodology to Determine Unsteady Pressure Loading on Components in Reactor Steam Domes (Rev. 6)." C.D.I. Report No. 04-09 (Proprietary).
2. Continuum Dynamics, Inc. (2007). "Acoustic and Low Frequency Hydrodynamic Loads at CLTP Power Level on Browns Ferry Nuclear Unit 2 Steam Dryer to 250 Hz with Noise Removed" C.D.I. Report No. 08-05P (Proprietary)
3. Continuum Dynamics, Inc. (2007). "Acoustic and Low Frequency Hydrodynamic Loads at CLTP Power Level on Browns Ferry Nuclear Unit 2 Steam Dryer to 250 Hz with Noise Removed" C.D.I. Report No. 08-05P (Proprietary)
4. Structural Integrity Associates, Inc. (2006). "Main Steam Line 100% CLTP Strain Data Transmission." SIA Letter Report No. GSZ-06-017.
5. ANSYS Release 10.0. URL <http://www.ansys.com>. Documentation: ANSYS 10.0 Complete User's Manual Set
6. Continuum Dynamics, Inc. (2007). "Stress Assessment of Browns Ferry Nuclear Unit 1 Steam Dryer, Rev. 0," C.D.I. Report No. 08-06P (Proprietary).
7. Press, W. H., S. A. Teukolsky, et al. (1992). *Numerical Recipes*, Cambridge University Press.
8. O'Donnell W.J. (1973). "Effective Elastic Constants For the Bending of Thin Perforated Plates With Triangular and Square Penetration Patterns," ASME Journal of Engineering for Industry, Vol. 95, pp. 121-128.
9. Idel'chik, I E. and Fried, E. (1989). *Flow Resistance, a Design Guide for Engineers*, Taylor & Francis, Washington D.C., p 260.
10. DeSanto, D.F. (1981). "Added Mass and Hydrodynamic Damping of Perforated Plates Vibrating in Water," Journal of Pressure Vessel Technology, Vol. 103, p. 176-182.
11. Continuum Dynamics, Inc. (2007). "Dynamics of BWR Steam Dryer Components," C.D.I. Report No. 07-11P
12. U.S. Nuclear Regulatory Commission, (2007). Regulatory Guide 1.20 "Comprehensive Vibration Assessment Program for Reactor Internals During Preoperational and Initial Startup Testing," March 2007.
13. WRC Bulletin 432 (1998). "Fatigue Strength Reduction and Stress Concentration Factors For Welds In Pressure Vessels and Piping," WRC, NY, p.32
14. Pilkey W.D. (1997). *Peterson's Stress Concentration Factors*, 2nd ed., John Wiley, NY, p.139.

15. Lawrence F.V., Ho N.-J., Mazumdar P.K. (1981). "Predicting the Fatigue Resistance of Welds," *Ann. Rev. Mater. Sci.*, vol. 11, pp. 401-425.
16. General Electric (GE) Nuclear Energy (2003). Supplement 1 to Service Information Letter (SIL) 644, "BWR/3 Steam Dryer Failure," September 5, 2003.
17. Tecplot 10 (2004). URL: <http://www.tecplot.com>. Documentation: *Tecplot User's Manual* Version 10 Tecplot, Inc. Bellevue, Washington October.